




# Osteocyte *Sptbn1* Deficiency Alters Cell Survival and Mechanotransduction Following Formation of Plasma Membrane Disruptions (PMD) from Mechanical Loading

Mackenzie L. Hagan<sup>1</sup> · Anik Tuladhar<sup>1</sup> · Kanglun Yu<sup>1</sup> · Dima W. Alhamad<sup>1</sup> · Husam Bensreti<sup>1</sup> · Jennifer Dorn<sup>1</sup> · Victor M. Piedra<sup>1</sup> · Nicholas Cantu<sup>1</sup> · Eric G. Stokes<sup>1</sup> · Daniel Blumenthal<sup>1</sup> · Rachel L. Roberts<sup>1</sup> · Vanshika Balayan<sup>1</sup> · Sarah M. Bass<sup>1</sup> · Thomas Dickerson<sup>1</sup> · Anabel Liyen Cartelle<sup>1</sup> · Marlian Montesinos-Cartagena<sup>1</sup> · Mohamed E. Awad<sup>2</sup> · Alberto A. Castro<sup>3</sup> · Theodore Garland Jr.<sup>3</sup> · Marion A. Cooley<sup>2</sup> · Maribeth Johnson<sup>4</sup> · Mark W. Hamrick<sup>1</sup> · Paul L. McNeil<sup>1</sup> · Meghan E. McGee-Lawrence<sup>1,5</sup> 

Received: 16 May 2024 / Accepted: 30 August 2024

© The Author(s), under exclusive licence to Springer Science+Business Media, LLC, part of Springer Nature 2024

## Abstract

We and others have shown that application of high-level mechanical loading promotes the formation of transient plasma membrane disruptions (PMD) which initiate mechanotransduction. We hypothesized that increasing osteocyte cell membrane fragility, by disrupting the cytoskeleton-associated protein  $\beta$ 2-spectrin (Sptbn1), could alter osteocytic responses and bone adaptation to loading in a PMD-related fashion. In MLO-Y4 cells, treatment with the spectrin-disrupting agent diamide or knockdown of Sptbn1 via siRNA increased the number of PMD formed by fluid shear stress. Primary osteocytes from an osteocyte-targeted DMP1-Cre Sptbn1 conditional knockout (CKO) model mimicked trends seen with diamide and siRNA treatment and suggested the creation of larger PMD, which repaired more slowly, for a given level of stimulus. Post-wounding cell survival was impaired in all three models, and calcium signaling responses from the wounded osteocyte were mildly altered in Sptbn1 CKO cultures. Although Sptbn1 CKO mice did not demonstrate an altered skeletal phenotype as compared to WT littermates under baseline conditions, they showed a blunted increase in cortical thickness when subjected to an osteogenic tibial loading protocol as well as evidence of increased osteocyte death (increased lacunar vacancy) in the loaded limb after 2 weeks of loading. The impaired post-wounding cell viability and impaired bone adaptation seen with Sptbn1 disruption support the existence of an important role for Sptbn1, and PMD formation, in osteocyte mechanotransduction and bone adaptation to mechanical loading.

**Keywords** Osteocyte ·  $\beta$ 2-Spectrin · Mechanotransduction · Plasma membrane · Mechanical loading

## Introduction

Osteocytes embedded within the bone extracellular matrix sense mechanical loads placed on the skeleton and direct downstream adaptation via signaling to osteoblasts and osteoclasts, where higher-level impact loads induce a greater osteogenic response as compared to more gradual application of loading [1–5]. Although fluid flow shear stress has been identified as a key component of osteocyte mechanosensation, the precise molecular mechanisms that osteocytes use to detect mechanical stimuli are still being elucidated. In vitro studies have shown strong support for the relevance of gap junctions and Connexin43 hemichannels [6–12], integrins [13, 14], TRPV4 channels and microtubules [15], and Piezo channels [16] in processes of osteocyte

✉ Meghan E. McGee-Lawrence  
mmcgeelawrence@augusta.edu

<sup>1</sup> Department of Cellular Biology and Anatomy, Medical College of Georgia, Augusta University, 1460 Laney Walker Blvd, CB1101, Augusta, GA 30912, USA

<sup>2</sup> Department of Oral Biology and Diagnostic Sciences, Dental College of Georgia, Augusta University, Augusta, GA, USA

<sup>3</sup> Evolution Ecology & Organismal Biology Department, University of California Riverside, Riverside, USA

<sup>4</sup> Department of Neuroscience and Regenerative Medicine, Medical College of Georgia, Augusta University, Augusta, GA, USA

<sup>5</sup> Department of Orthopaedic Surgery, Augusta University, Augusta, GA, USA

mechanosensation. However, none of these mechanisms have yet fully explained how osteocytes sense and respond to higher levels (e.g., impact loads) of mechanical stimuli *in vivo*. We believe osteocytes utilize the proposed methods above, but in addition, develop small, repairable plasma membrane disruptions (PMD) both *in vitro* and *in vivo* in response to higher levels of mechanical loading [17–21], and that these PMD may serve as an additional mechanosensation mechanism for osteocytes at these high levels of load (e.g., > 30 dynes/cm<sup>2</sup>). Osteocyte PMD formation likely occurs via drag forces applied to the osteocyte pericellular matrix around dendrites during loading-induced fluid shear [20]. However, the relative importance of PMD in osteocyte mechanosensation and subsequent bone adaptation has not been rigorously tested.

Mechanosensitive tissues, such as epithelial cells and myocytes, also develop PMD with mechanical loading and show evidence of mechanotransduction downstream of these PMD [22–31]. Importantly, previous studies in such tissues revealed that one effective strategy to test PMD relevance in mechanosensation is to alter PMD susceptibility and observe downstream effects on associated tissue adaptation. For example, in myocytes, absence of the cytoskeletal structural protein dystrophin promoted increased PMD formation both under normal loading conditions (e.g., normal cage activity) and with exposure to exercise [32]. The absence of dystrophin in mice (e.g., the *mdx* mouse model) increased the fragility of the myocyte plasma membranes, resulting in the formation of more frequent, larger plasma membrane disruptions that were more difficult to repair and survive [32]. Ultimately, this promoted atrophy of the tissue as the progenitor cell pool used to replenish lost myocytes became depleted. These observations led us to the question whether modulating plasma membrane integrity in osteocytes would affect PMD development and subsequent downstream bone adaptation to mechanical loading.

Although osteocytes do not express dystrophin, they do abundantly express the structurally similar protein non-erythrocytic 1 spectrin  $\beta$  (also known as  $\beta$ II spectrin, a product of the *Sptbn1* gene). This protein is particularly prevalent in the dendritic processes that are important for detection of mechanical loading [7, 33, 34]. Members of the spectrin super-family of proteins, such as *Sptbn1* and dystrophin, bind F-actin to ankyrin to provide structural support to the plasma membrane. *Sptbn1* has already been implicated as an important mediator of skeletal health, as polymorphisms in the *SPTBN1* locus were linked to low bone mineral density (BMD) and fracture risk in several human genome-wide association studies (GWAS) [35–37]. The molecular mechanisms behind this association are not currently known. We hypothesized that disrupting the osteocyte spectrin network would lead to increased osteocyte membrane fragility, resulting in greater susceptibility to

PMD formation, allowing a mechanistic investigation into the effect of PMD in osteocytic responses to mechanical loading and subsequent bone adaptation. We used genetic and pharmacological approaches to disrupt *Sptbn1* both *in vitro* and *in vivo*, testing the effect of these manipulations on osteocyte PMD formation, repair rate, post-wounding survival, and responses to loading.

## Materials and Methods

### Sptbn1 CKO Mouse Model

All animal experiments followed NIH guidelines and were approved by the Institutional Animal Care and Use Committee at Augusta University. Osteocyte-targeted male and female *Sptbn1* conditional knockout (CKO) mice were generated by crossing *Sptbn1* floxed mice (JAX #020288, exon 3 floxed) with the 10 kb DMP1-Cre mouse (JAX #023047) to generate *Sptbn1*<sup>fl/fl</sup>: Dmp1 Cre+ mice (hereafter referred to as *Sptbn1* CKO). Cre-negative *Sptbn1* floxed littermates (*Sptbn1*<sup>fl/fl</sup>: Dmp1-Cre-) served as wildtype littermate controls (hereafter referred to as WT). All mice were housed in standard rodent cages with a 12-hr light/ 12-hr dark schedule and were permitted water and standard rodent chow *ad libitum*.

### In Vitro Studies

#### Osteocyte Cell Culture

MLO-Y4 cells were maintained in growth medium ( $\alpha$ -MEM + 5% fetal bovine serum (FBS, Atlanta Biologicals) + 5% bovine calf serum (HyClone) + 1% Penicillin/Streptomycin). Primary osteocytes were isolated from long bone diaphyses (femur, tibia, and humerus) of *Sptbn1* CKO mice and WT littermates as described [20]. Cells were plated onto type 1 collagen-coated dishes and grown to 70% confluency, at which time cells were re-seeded for all subsequent experiments. All primary osteocyte experiments were conducted within 2 weeks of isolation, as recommended [38].

#### RNAscope Analysis of *Sptbn1* Expression

Deficiency in *Sptbn1* expression for the *Sptbn1* CKO model was confirmed in primary osteocytes via RNAscope. Primary osteocytes were grown in type 1 collagen coated 10 cm dishes then were seeded onto glass slides coated with type 1 collagen at a density of 40,000 cells/slide. Cells were grown for 4 days more days on the glass slides, then fixed with 4% formaldehyde, dehydrated, and stored in a – 20 °C freezer. On the day of the experiment, the slides were rehydrated and processed according to the protocol provided by Advanced

Cell Diagnostics (ACD). Briefly, the slides were exposed to hydrogen peroxide for 10 min, then protease III for 10 min. *Sptbn1* probe (#546,241) was added to the slides for 2 h in the HybEZ™ II oven. Slides were left overnight in 5× saline sodium citrate buffer. The next day, the signal was amplified using the RNAscope® Multiplex Fluorescent Reagent Kit v2 (#323,100). HRP-C1 was added for 15 min, followed by TSA Vivid™ Fluorophore 520 for 30 min, then by HRP blocker for 15 min. The nucleus was stained with Hoechst and slides were mounted using Vectamount aqueous mounting media (#101,098–068). Slides were imaged with a 40× objective using a Leica STELLARIS confocal microscope.

### Sptbn1 Disruption via Diamide Treatment and siRNA

To test the effects of *Sptbn1*-disruption in immortalized osteocytes, MLO-Y4 cells were treated with diamide (500 μM; 10 min prior to wounding) as previously described [34]. Effects of diamide treatment on the integrity of the spectrin network were assessed via immunocytochemical staining using a commercial antibody (anti-*Sptbn1*, abcam #ab72239). F-actin was visualized using TRITC-labeled phalloidin (Sigma #P1951) and nuclei were stained with DAPI. Maximum fluorescence intensity for each channel was calculated for individual cells. For siRNA studies, MLO-Y4 cells were transfected with an siRNA against *Sptbn1* (Santa Cruz #270,043) or a scrambled control (Santa Cruz #37,007) using a commercial transfection reagent (Lipofectamine RNAiMax; ThermoFisher Scientific #13,778,075). Studies were initiated 72 h after transfection.

### RNA Isolation and PCR Analysis

RNA was isolated from cell lysates as previously described [39]. Reverse transcription was performed using a commercially available reverse transcription kit (Invitrogen Superscript III), where the final concentration of cDNA was 2000 ng/μL. Semi-quantitative PCR (qPCR) was performed using SYBR green PCR kit (Qiagen Quantitect #204,143) on a BioRad CFX Connect PCR system. Each PCR reaction contained 37.5 ng cDNA. Primer sequences were as follows: *Gapdh*\_F: 5'-GGGAAGCCCATCACCATC-3', *Gapdh*\_R: 5'-GCCTACCCCATTTGATGTT-3', *Sptbn1*\_F: 5'-CAGCACCTTGGCCTCACTAA-3'; *Sptbn1*\_R: 5'-CCAATGCGCTTTCCTTCGAC-3'.

### Laser Wounding—Analysis of PMD Repair Rates

Osteocytes were seeded into 60 mm dishes in osteocyte culture medium and wounded with an 820 nm multiphoton laser in PBS containing calcium (1.8 mM) and FM1-43 dye (3 μM), as we previously described [21]. One PMD per osteocyte, located on a dendritic process, was created. To

estimate PMD size, FM1-43 dye influx was measured as area under the curve (AUC) over the first 40 s of the experiment (i.e., during the phase of exponential, rapid dye influx prior to plateau from repair) [20, 21]. To quantify PMD repair rate, the derivative of the FM1-43 fluorescence versus time curve was calculated to permit analysis of the curve slope, indicative of repair rate quantified as the AUC of this slope vs. time curve [20].

### Laser Wounding—Calcium Signaling

Osteocytes were loaded with Cal-520-AM dye (catalog # 171,868), after which calcium signaling was initiated by a laser-induced PMD as described [20]. Transmission of calcium signaling to non-wounded adjacent cells was quantified as previously described [20], measured as the number of non-wounded cells with Cal-520AM fluorescence exceeding background levels after laser firing and the AUC of the fluorescence vs. time curves for these non-wounded cells.

### Fluid Flow Shear Stress

Osteocytes were seeded into type 1 collagen-coated flow chamber slides (Ibidi, μSlide VI<sup>0.4</sup>, #80,606; 1,000 cells per channel) and cultured for up to 4 days with fresh media added daily. Cells were subjected to fluid flow shear stress (30 dynes/cm<sup>2</sup>) for 5 min using a syringe pump (Harvard Apparatus PHD Ultra I/W) and culture medium supplemented with 1 mg/ml of 10 kDa fluorescein-conjugated dextran used as a membrane disruption tracer, as previously described [21]. At the conclusion of experiments, cells were washed 3 times with PBS and imaged on a confocal microscope (Zeiss). Cytosolic retention of fluorescein dextran was interpreted as evidence of a membrane disruption event; wounded cells permit entry of the dextran molecule, and successful PMD repair seals the tracer inside the cell [21]. The percentage of wounded osteocytes normalized to total cell number was quantified in each experiment. Using parameters described above, varying sizes of fluorescently conjugated dextran (3 kDa, 10 kDa, 70 kDa) were added to the flow medium in replicate experiments to characterize approximate relative PMD size in primary osteocytes isolated from *Sptbn1* CKO and WT littermate mice. Three fluid flow shear stress intensities (10, 30, and 50 dynes/cm<sup>2</sup>) were independently tested for each size of dextran.

### Post-wounding Cell Survival

For assessment of post-wounding repair and survival, MLO-Y4 osteocytes were wounded by glass beads, as previously described [21] and primary osteocytes isolated from female *Sptbn1* CKO and WT mice were subjected to fluid shear as described above (30 dynes/cm<sup>2</sup>, 5 min). In both flow and

bead wounding conditions, cells were stained at least 5 min after wounding with propidium iodide (PI; 0.3  $\mu\text{g}/\text{mL}$ ) to detect dead cells (i.e., unrepaired PMD) and imaged on a confocal microscope (Zeiss) [21]. The percentages of dead cells (PI+) normalized to total cell number were quantified with image analysis software (Bioquant).

## In vivo Studies

### Establishment of Voluntary Wheel Running and Uniaxial Tibial Loading Models in Wildtype Mice

Building upon our previous work using treadmill models, before testing the role of *Sptbn1* in osteocyte responses to loading, we wanted to establish which forms of mechanical loading promoted osteocyte PMD formation in mice. We first tested voluntary wheel running, which (like downhill treadmill exercise) has been reported to increase PMD formation in *mdx* mice [40]. As proof of principle, these studies were conducted on mice selectively bred for high voluntary wheel-running activity as well as non-selected control lines. At generation 80, we sampled male and female mice from each of four different “High Runner” mouse lines that had been selectively bred to have high voluntary wheel-running activity and from four non-selected control mouse lines (“Control”) as previously described [41, 42]. At 12 weeks of age, beginning six days prior to sacrifice, half of the animals within each group were provided access to a running wheel (Wahman-type activity wheels, 1.12 m circumference, 35.7 cm diameter, 10 cm wide running surface) that permitted voluntary running for 6 days while the remaining mice had no wheel access. All animals received sequential subcutaneous injections of calcein 5 days and 1 day prior to sacrifice to label mineralizing bone surfaces.

As a second model, given recent concerns about off-target expression of *Dmp1-Cre* in skeletal muscle [43], we established a uniaxial tibial loading protocol which would not require skeletal muscle contraction to induce bone loading. Female CD-1 wildtype mice were subjected to either one bout (acute) or 2 weeks (chronic) of uniaxial tibial loading as previously described [44–46] beginning at 12 weeks of age. Chronic loading of the left tibia was performed three days per week on alternating days; the right tibia for each mouse served as a non-loaded internal control. Mice were anesthetized with isoflurane, and each loading session consisted of 50 loading cycles with a linear ramp to a peak of -11 N ( $\sim 1500\mu\text{e}$ , based on preliminary strain gauging studies; *data not shown*), 0.2 s dwell followed by a linear release at the same rate and another dwell near zero load for 10 s before the next cycle. All animals received sequential subcutaneous injections of calcein on days 5 and 1 prior to sacrifice to label mineralizing bone surfaces. Mice were sacrificed via

carbon dioxide and were immediately perfused with 10% formalin prior to tissue harvest.

### Tibial Loading Studies in the *Sptbn1* CKO Mouse Line

*Sptbn1* CKO mice and littermate controls were subjected to either one bout (acute) or 2 weeks (chronic) of uniaxial tibial loading as described above and were administered subcutaneous injections of alizarin complexone 5 days and 1 day prior to sacrifice to label mineralizing bone surfaces for dynamic histomorphometry studies.

### Osteocyte PMD Formation from Acute Loading

Plasma membrane disruptions were detected in the tibiae of mice subjected to wheel running or tibial loading as previously described [19–21]. Bones were decalcified in 15% EDTA, paraffin embedded, sectioned longitudinally, and subjected to immunohistochemistry with a FITC-conjugated mouse albumin antibody (AIFAG3140, Accurate Chemical Corp.) to detect cytoplasmic localization of endogenous albumin as a PMD tracer [19–21]. Sections were counterstained with DAPI (Vectashield) to visualize cell nuclei. Osteocytes presenting with a signal for both DAPI and cytosolic albumin labeling were interpreted as having experienced a PMD. Five images per bone were captured (Zeiss LSM780) and analyzed with Bioquant Osteo (Nashville, TN) to quantify the relative percentage of PMD-labeled osteocytes for each bone.

### DXA and Micro-computed Tomography (microCT) Analysis of Cortical Bone Geometry

*Sptbn1* CKO mice and littermate WT controls were subjected to dual-energy X-ray absorptiometry (DXA; Kubtec Digimus software) analysis for quantification of whole body bone mineral density (BMD) at 1 month and 5 months of age under isoflurane anesthesia as previously described [47, 48] to determine whether conditional depletion of *Sptbn1* in osteocytes induced a developmental phenotype. BMD was also assessed in isolated tibiae collected from the wheel-running High Runner and Control mice; bones were sandwiched between two thin strips of silicone (Walgreens Silicone Scar Sheets) to attenuate x-rays in the absence of overlying soft tissue.

Cortical bone architecture was analyzed in mid-diaphysis of the tibia (proximal to tibia-fibula junction; CD-1 mice and *Sptbn1* CKO and WT mice subjected to tibial loading) or mid-diaphysis of the femur (developmental phenotype of *Sptbn1* CKO mice) by ex vivo  $\mu\text{CT}$  (Skyscan 1272), as previously described [19, 49]. Scanning parameters were as follows: source voltage = 70 kV, source current = 142  $\mu\text{A}$ , exposure 897 ms/frame, average of 3 frames per projection,

rotation step = 0.600 degrees and 0.25 mm aluminum filter. The specimens were scanned at high resolution (1224 × 820 pixels) with an isotropic voxel size of 9.49 μm. Reconstructions for X-ray projections were performed using the Bruker micro-CT Skyscan software (NRecon, and DataViewer) (v. 1.7.3.1, Bruker micro-CT, Kontich, Belgium). Ring artifact and beam hardening corrections were applied in reconstruction. Datasets were loaded into CTAnalyser software vs. 1.20.3.0 (Skyscan) and region and volume of interest were selected from the reconstructed image stacks. Properties (9–13 μm/voxel resolution) were calculated with the manufacturer's software. For the wheel-running High Runner and Control mice, the mid-diaphysis of each femur was analyzed for a subset of mice by micro-computed tomography (Skyscan 1174, 19 μm resolution), and cortical bone properties were quantified with the manufacturer's software (CTAn) as described above.

### Dynamic Histomorphometry Analysis of Cortical Bone Formation

Bones were embedded in methyl methacrylate for dynamic histomorphometry as previously described [50]. Briefly, cross-sections were cut from the mid-diaphysis with a low-speed diamond saw (Buehler Isomet) and hand polished on a grinding wheel (Buehler Ecomet) as needed to < 100 μm thickness. Sections were mounted on glass slides (Cytoseal™ XYL) and imaged with an epifluorescent microscope (Olympus IX-70) and digital camera (QIcam). Periosteal and endocortical mineral apposition rates (MAR, μm/day) and mineralizing surfaces (MS/BS, %) were quantified with image analysis software (Bioquant OSTEO, Nashville TN) as previously described [50, 51].

### Lacunar Occupancy

Thin (10 μm) longitudinal tibial sections were obtained from the methyl methacrylate blocks of the mice subjected to 2 weeks of tibial loading and from the paraffin blocks of mice subjected to one bout of acute loading. Sections were stained with Goldner's Trichrome to determine osteocyte lacunar vacancy as a measure of cell viability as previously described [50]. Bone sections were examined at 400 × magnification, and a total of 10 images per bone were collected at random locations throughout the cortical bone. The percentage of empty osteocyte lacunae was quantified with image analysis software (Bioquant Osteo).

### Statistics

For all datasets, sample sizes for each experiment are described in the respective figure legends and tables. Datasets with two conditions were analyzed by pooled *t* tests or

matched pair *t*-tests (the latter used when comparing loading responses between loaded vs. non-loaded limbs within the same mouse). For tibial loading studies in the *Sptbn1* CKO mouse line, the percent difference in each bone property measured by microCT and dynamic histomorphometry between the loaded left tibia and the non-loaded right tibia was calculated for each mouse as: % difference =  $[\text{bone property}_{\text{lefttibia}} - \text{bone property}_{\text{righttibia}}] / \text{bone property}_{\text{righttibia}}$  (where *bone property* = cortical bone area, cortical bone thickness, etc.) to assess relative changes in bone properties with loading. Datasets with more than two conditions were analyzed by ANOVA with interaction effects followed by Fisher's LSD post hoc tests as appropriate. JMP Pro statistical analysis software (v. 17.0.0; SAS Institute) was used for all analyses and alpha = 0.05 used to determine statistical significance. Grubb's extreme studentized deviate test (GraphPad) was used to exclude a maximum of one extreme outlier per group as needed [52].

For the wheel-running experiments with High Runner and Control lines of mice, with the exception of microCT datasets (which were not available for mice from every line), data were analyzed as mixed models in SAS procedure MIXED with restricted maximum likelihood estimation and Type III tests of fixed effects (e.g., [41, 42, 53]). Selection for High Runner characteristics (Selection or "Linetype"; HR vs. C), sex, and mini-muscle status (see below) were fixed main effects. Replicate line was a random effect nested within linetype. All of these main effects and their interactions were tested relative to the variance among lines, with 1 and 6 degrees of freedom (df), as dictated by the design of the selection experiment. Mini-muscle status was tested relative to the residual df. As previously described, the mini-muscle phenotype is characterized primarily by a 50% reduction in hind limb muscle mass [54, 55]. The underlying genetic variant is a C-to-T transition located in a 709-bp intron between exons 11 and 12 of the Myosin heavy polypeptide 4 gene [56] that behaves as a simple Mendelian recessive [54]. Mini-muscle status was determined based on a comparison of triceps surae muscle masses in relation to body mass [54]. As our primary focus was determining effects of wheel access and possible differences between High Runner and Control lines, we do not discuss mini-muscle effects in the text. However, all statistical results can be found in Supplemental Table 2.

## Results

### Validation of Osteocyte *Sptbn1*-Disrupting Strategies

Before testing the role of *Sptbn1* in osteocyte PMD formation and osteocytic responses to loading, we first examined

the efficacy of our intended strategies for disrupting Sptbn1 in osteocytes. While we first attempted western blotting for  $\beta$ II-spectrin protein levels in lysates from primary osteocytes isolated from Sptbn1 CKO and WT littermate mice,  $\beta$ II-spectrin is a large molecular weight protein (~274 kDa), and we encountered difficulty in consistently detecting proteins of this size on western blots (data not shown). However, primary osteocytes isolated from the Sptbn1 CKO mice showed a reduction in Sptbn1 mRNA signal as visualized by RNAscope as compared to primary osteocytes from WT littermates (Fig. 1A). Similarly, RNA isolated from MLO-Y4 cells treated with a Sptbn1 siRNA (72 h after transfection) showed a significant reduction in Sptbn1 gene expression by qPCR as compared to either un-transfected controls or cells transfected with a scrambled control siRNA ( $p < 0.0001$ ; Fig. 1B). We also employed a pharmacological approach,

subjecting MLO-Y4 cells to treatment with diamide (a thiol-oxidizing agent known to disrupt the spectrin network) which significantly reduced the immunohistochemical staining fluorescence intensity for Sptbn1 as previously reported [34] (Fig. 1C-D).

### Disruption of the Osteocyte Spectrin Network Increased the Relative Abundance and Size of Osteocyte PMD Formation During In Vitro Loading

To assess in vitro osteocyte PMD formation under mechanical loading conditions, osteocytes were exposed to fluid flow shear stress at 30 dynes/cm<sup>2</sup> in the presence of a membrane impermeant fluorescent dextran tracer (FDx; 10 kDa). Cells were grown for at least 2 days prior to experiments

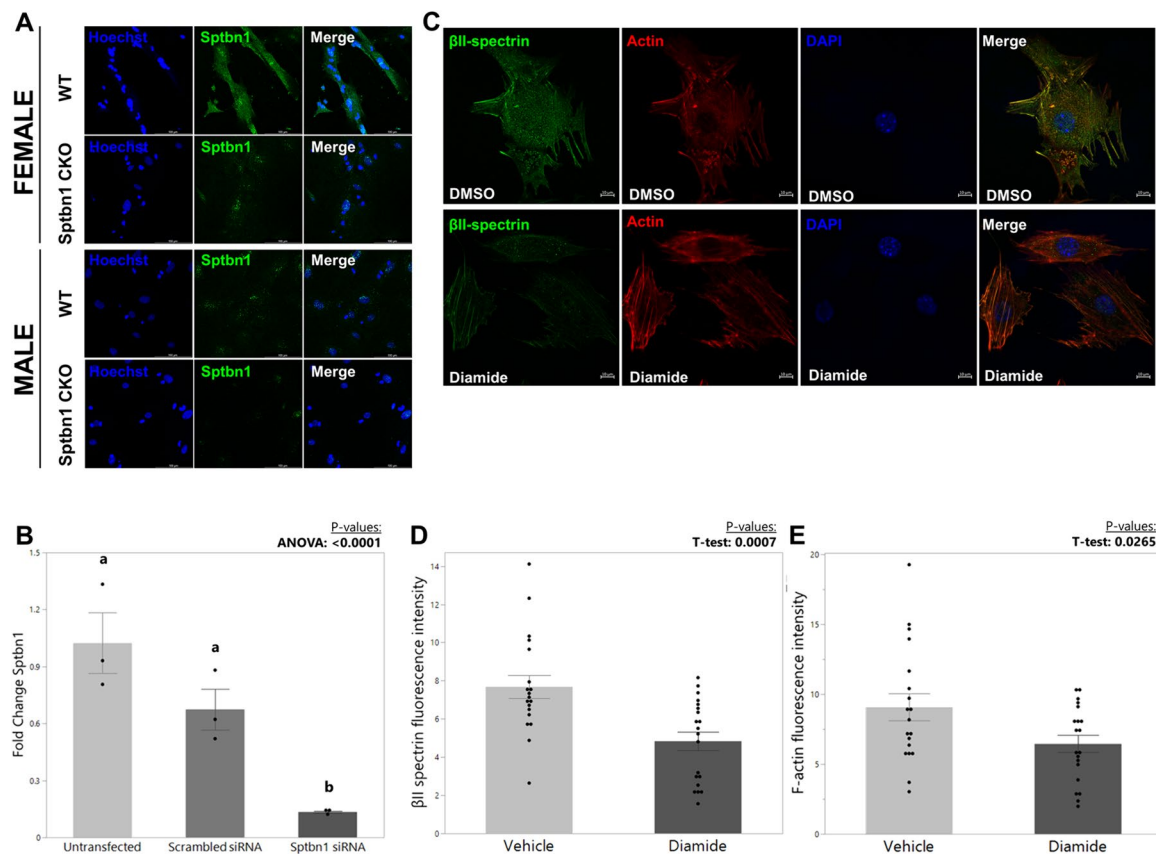


**Fig. 1** Validation of Sptbn1 disrupting strategies for in vitro studies. **A** Primary osteocytes isolated from male and female Sptbn1 CKO mice demonstrated a lower signal for Sptbn1 mRNA (green) in RNAscope analyses as compared to osteocytes from WT littermates. Cultures were imaged with a 40X objective; scale bar in each image equals 100  $\mu$ m. Images are representative of at least 3 replicates for each sex and genotype. **B** Treatment with Sptbn1 siRNA significantly reduced Sptbn1 mRNA expression in MLO-Y4 osteocytes. Groups were compared with 1-way ANOVA and Fisher's LSD post hoc tests. Bars in graphs show mean  $\pm$  SEM for each group, and each black circle represents an independent biological replicate culture; bars with

different superscript letters are significantly ( $p < 0.05$ ) different from one another as determined by post hoc testing. **C** Treatment of MLO-Y4 osteocytes with the thiol-oxidizing agent diamide disrupted the immunocytochemical signature for  $\beta$ II-spectrin. Images are representative of at least 3 replicate cultures. **D, E** The maximum fluorescent intensity for **D**  $\beta$ II-spectrin and **E** F-actin (as shown by phalloidin staining) were quantified using Zen image analysis software. Groups were compared with *t* tests; Bars in graphs show mean  $\pm$  SEM for each group and each black circle represents one cell across three independent biological replicate experiments

to promote the formation of a pericellular matrix [20]. As we previously observed no uptake of PMD tracers in the absence of applied shear stress [21], cells were only imaged at the conclusion of loading. MLO-Y4 osteocytes treated with diamide (Fig. 2A) or *Sptbn1* siRNA (Fig. 2B) displayed significantly more PMD following 5 min of exposure to fluid shear. Studies were repeated using primary osteocytes isolated from *Sptbn1* CKO and WT littermate mice, where we employed three shear stress rates (10 dynes/cm<sup>2</sup>, 30 dynes/cm<sup>2</sup>, and 50 dynes/cm<sup>2</sup>) as well as three different sizes of fluorescent dextran molecules (3 kDa, 10 kDa, and 70 kDa)

in an effort to assess the impact of *Sptbn1* knockdown on PMD size, represented by the relative size of the tracer able to enter the cell under each flow profile as described in previous studies [17, 18]. Using methodology previously described to estimate the molecular radius of each fluorescent tracer [18, 57], we estimated that the molecular radii of 3, 10, and 70 kDa dextran molecules (reflective of the PMD size necessary to permit these dyes to enter the cell) were 0.95 nm, 1.42 nm, and 2.72 nm, respectively. As seen with diamide and *Sptbn1* siRNA, primary osteocytes from *Sptbn1* CKO mice developed more osteocyte PMD with shear stress

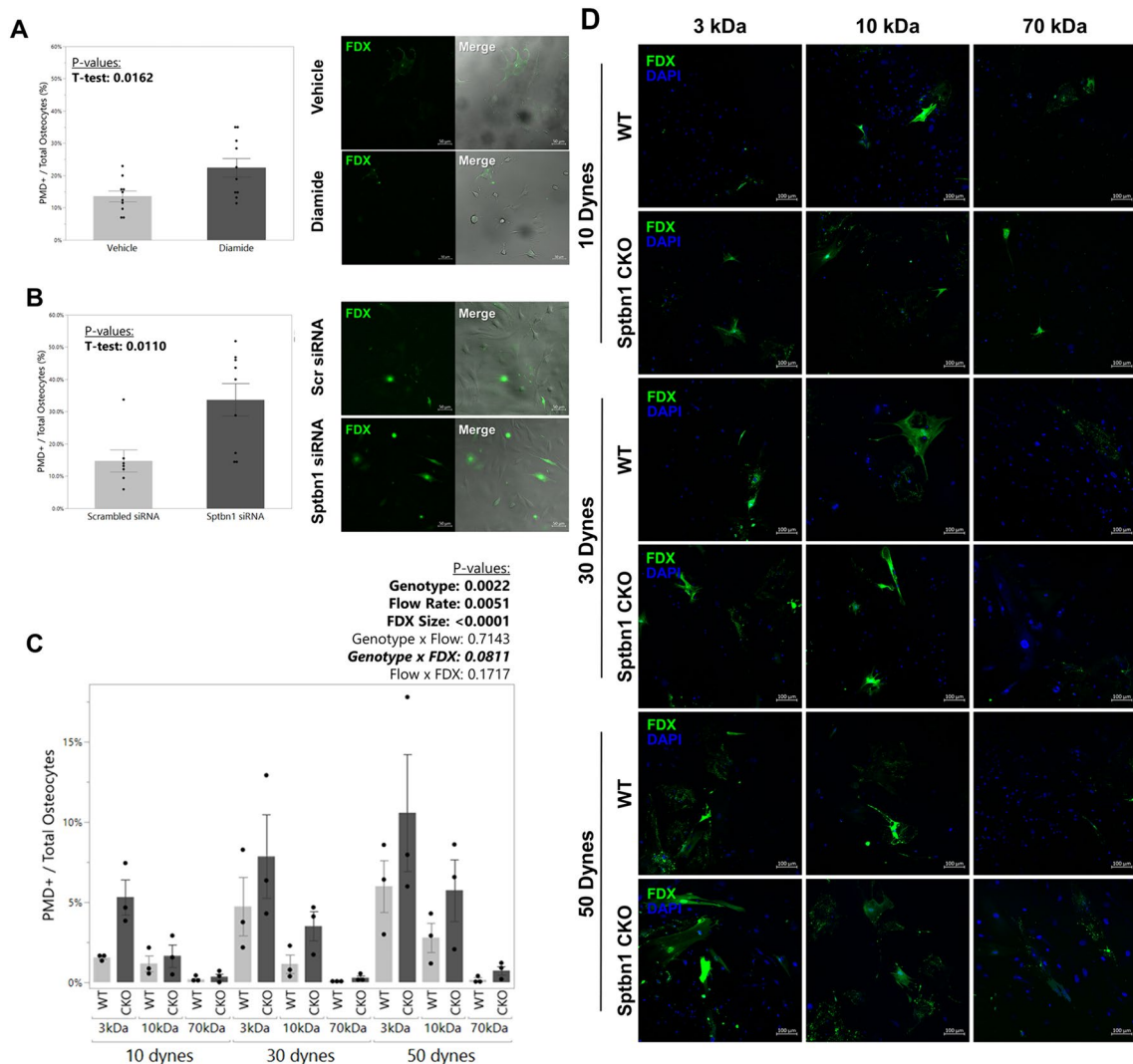


**Fig. 2** Osteocyte PMD formation is enhanced following *Sptbn1* disruption in vitro. Treatment of MLO-Y4 osteocytes with **A** diamide or **B** siRNA against *Sptbn1* significantly increased the number of cells with PMD, measured as cytosolic localization of 10 kDa dextran following 5 min of fluid shear (30 dynes/cm<sup>2</sup>) as compared to control cultures. Representative images from each experiment are shown next to the quantitative graph. **C** Primary osteocytes isolated from *Sptbn1* CKO mice demonstrated a significant increase in the number of cells with cytosolic localization of dextran (p<sub>genotype</sub>=0.0022) follow-

ing 5 min of fluid shear (10–50 dynes/cm<sup>2</sup>) as compared to control cultures. A trend for an interaction effect between genotype and dextran size (p<sub>genotype x FDX</sub>=0.081) suggested a tendency for larger sizes of dextran to enter *Sptbn1* CKO osteocytes at a given level of loading as compared to WT cells. **D**) Representative images from experiments in Panel C. FDX: fluorescent dextran (3, 10, 70 kDa as indicated by the column title), DAPI (blue)=nucleus. Bars in graphs show mean ± SEM for each group and each black circle represents an independent biological replicate

( $p_{\text{genotype}} = 0.0022$ ) (Fig. 2C, D), suggestive of increased susceptibility to PMD formation. Flow rate was also associated with PMD abundance, with more PMD occurring at higher levels of shear stress as we previously reported ( $p_{\text{Flow Rate}} = 0.0051$ ) [21], whereas dextran tracer size was inversely related to PMD abundance ( $p_{\text{FDX Size}} < 0.0001$ ), with few osteocytes showing intracellular presence of the 70 kDa tracer after flow even at the highest levels of shear (Fig. 2C, D); this latter result suggests that the majority of PMD formed at these shear levels have a radius of less than 2.7 nm in size, as they did not permit entry of the 70 kDa tracer. However, we observed a trend for an interaction between genotype and dextran size ( $p_{\text{Genotype} \times \text{FDX}} = 0.0811$ ); this result suggests that the Sptbn1 CKO cultures tended to show greater intracellular presence of the larger fluorescent dextran molecules for a given level of shear stress, suggesting the possibility of increased PMD size in Sptbn1 CKO as compared to WT osteocytes (Fig. 2C, D).

### PMD Repair Rate was Slower in Sptbn1-Targeted Osteocytes

Given the data suggesting increased susceptibility and size of osteocyte PMD in the Sptbn1-disrupted osteocytes, we quantified PMD repair rates using previously established methodology [20, 21, 50]. Consistent with the idea of increased PMD size with Sptbn1 disruption seen in fluid shear stress studies, we observed a trend for increased FM1-43 dye influx immediately after creation of laser-induced PMD (as measured by area under the curve) in Sptbn1 CKO osteocytes ( $p_{\text{genotype}} = 0.0779$ ) as compared to WT controls in laser wounding experiments, specifically in the first 40 s after wounding (Fig. 3A). Increased influx of FM1-43 in the earliest time points of the laser wounding experiment suggests rapid influx of membrane-impermeant dye consistent with the formation of a larger PMD. The derivative of the FM1-43 fluorescence versus time curve was calculated to permit analysis of the curve slope, indicative of repair rate, which was quantified as the AUC of this slope vs. time curve as described in our previous studies [20]. The area under the curve of these slope vs. time graphs was significantly increased in the Sptbn1 CKO osteocytes ( $p_{\text{genotype}} = 0.0442$ ), indicative of a slower rate of PMD repair (Fig. 3B).

### Post-wounding Cell Survival was Decreased with Sptbn1 Disruption

Slow PMD repair can promote post-wounding cell death [20, 50]. To test whether the increased susceptibility to PMD, larger PMD size, and/or slower repair would impact post-wounding cell survival, we employed a mechanical wounding assay with glass beads. Cells were stained with propidium iodide after wounding to detect non-repaired

(i.e., dead) cells. Diamide treatment significantly increased the number of osteocytes that did not survive the wounding event (Fig. 4A). Notably, diamide in the absence of wounding did not increase cell death in these experiments, further supporting the idea that PMD repair failure, rather than an overall toxic effect of this drug, promoted cell loss (Fig. 4A). Comparable results were obtained with MLOY4 cells treated with Sptbn1-targeting siRNA and primary osteocytes isolated from Sptbn1 CKO mice subjected to fluid shear (Fig. 4B, C), where little to no evidence of cell death was seen in the absence of wounding (*data not shown*). Together, these results parallel the wounding-induced loss of myocyte viability seen in the *mdx* murine model of muscular dystrophy, which is deficient in the spectrin-family member dystrophin [32, 58–60].

### Calcium wave Propagation from Sptbn1 CKO Osteocytes was Minimally Affected

Evidence of mildly altered mechanotransduction was observed as a trend for diminished calcium signaling intensity in wounded cells from Sptbn1 CKO as compared to WT cultures ( $p_{\text{genotype}} = 0.0901$ ; Fig. 5A). We also observed a trend for the Sptbn1 CKO cultures to show an increased proportion of non-wounded neighboring cells initiating calcium signaling following creation of a single PMD in a nearby cell (Fig. 6B,  $p_{\text{genotype}} = 0.0774$ ) and for increased calcium signaling intensity in the non-wounded neighboring cells ( $p_{\text{genotype}} = 0.0523$ ). This observation may be consistent with the increased PMD size and slower rate of PMD repair in the Sptbn1 CKO cultures, as previous studies have shown that PMD repair rate is inversely proportional to the amount of ATP released from a wounded osteocyte [17, 18], but we wish to clearly acknowledge the limitation that none of these experiments reached our threshold to be considered statistically significant ( $p < 0.05$ ).

### Osteocytes from Wildtype Mice Developed PMD from Voluntary Wheel Running and Uniaxial Tibial Loading In Vivo

We previously investigated osteocyte PMD formed in wildtype mice during forced downhill treadmill running [20, 21, 50], which is a loading model reported to cause acute myocyte damage in mice that are deficient in the spectrin family member dystrophin (i.e., *mdx* mouse model) [61, 62]. However, we recognized that this loading model has inherent limitations such as its damaging nature and varied effects on bone [63–66], and therefore before investigating the effects of Sptbn1 in osteocyte PMD formation in vivo, we first tested whether other forms of mechanical loading could be used to promote osteocyte PMD formation using wildtype mice. We first tested voluntary wheel running, which (like



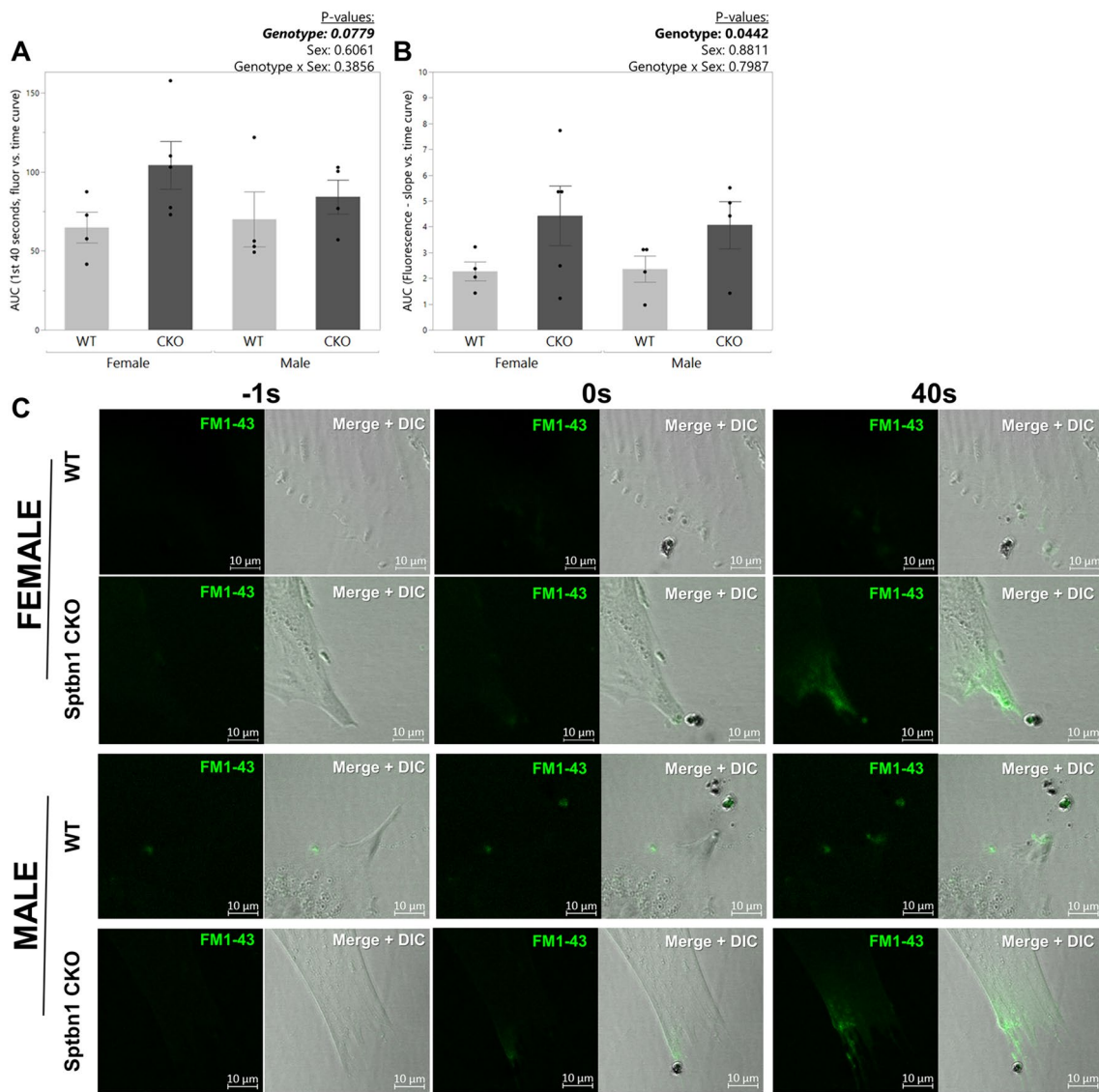


**Fig. 3** **A** Primary osteocytes isolated from *Sptbn1* CKO mice demonstrated a trend for greater FM1-43 dye influx immediately following creation of a PMD in laser wounding experiments, suggestive of increased PMD size. Bars in graph show mean  $\pm$  SEM for each group; each black circle represents an independent biological replicate culture. **B** The derivative (slopes) of the FM1-43 fluorescence versus time curves from laser wounding assays was plotted and area under the curve (AUC) quantified to measure PMD repair rate; these data suggested significantly slower rates of membrane repair in

osteocytes from *Sptbn1* CKO as compared to WT littermates, as seen by a significant effect of genotype in 2-factor ANOVA analyses ( $p=0.044$ ) for AUC. Bars in graph show mean  $\pm$  SEM for each group; each black circle represents an independent biological replicate culture. **C** Representative images from the experiments in Panels A and B, FM1-43 dye can be seen as an intracellular green fluorescent signal. A fluorescent image and a merged fluorescent + DIC (transmitted light) image is shown for each condition

downhill treadmill exercise) has been reported to increase PMD formation in *mdx* mice [40]. These experiments were performed using a previously established “High Runner” wildtype mouse model along with non-selected controls [41, 42], as reliable wheel running performance was previously established in this model. Although a baseline level of osteocyte PMD was detected in the tibia of mice with no wheel access, both the Control and High Runner groups showed a significant increase in the percentage of osteocyte PMD in

mice with access to a wheel as compared to no wheel access ( $p_{\text{wheel}}=0.0396$ ; Fig. 6A, B). No differences were observed between Control and High Runner groups in terms of tibial PMD abundance ( $p_{\text{selection}}=0.4962$ ); however, there was a trend for an interaction effect between wheel access and sex ( $p_{\text{wheel} \times \text{sex}}=0.0779$ ), with female mice tending to show more PMD with wheel access than males (Fig. 6A, B), consistent with the observation that female HR mice tend to run longer distances and at higher speeds than HR males [41, 67]. No

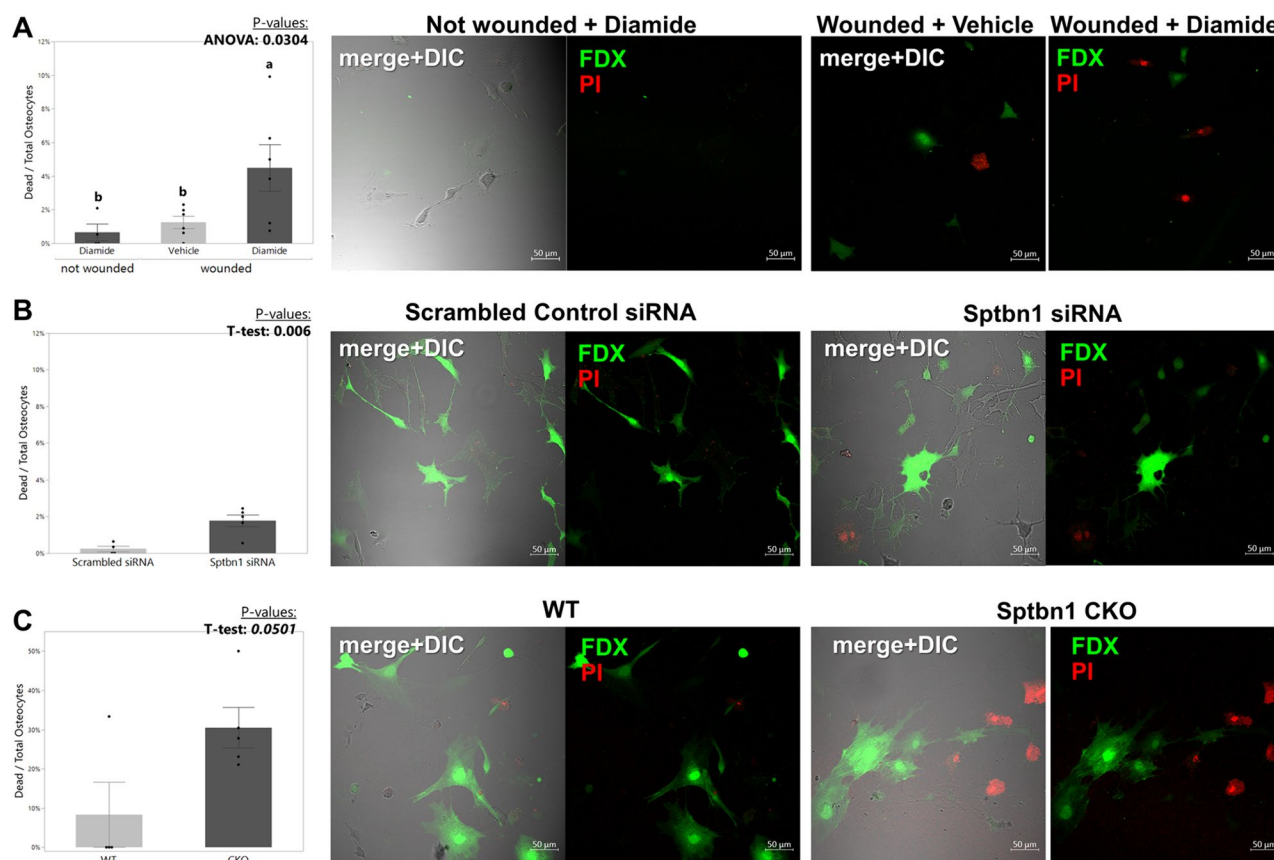


**Fig. 4** Sptbn1 disruption decreased post-wounding osteocyte survival. **A** The combination of bead wounding and diamide treatment, but not diamide alone, promoted cell death in MLO-Y4 osteocytes as seen by increased propidium iodide (PI; red) staining. Bars in graph show mean  $\pm$  SEM of independent biological replicate cultures and each black circle represents an independent biological replicate experiment; groups were compared by one-way ANOVA and Fisher's LSD post hoc testing. Bars with different superscript letters are significantly ( $p < 0.05$ ) different from one another. FDX: 10 kDa

fluorescent dextran. **B** Sptbn1 knockdown by siRNA promoted increased post-wounding cell death in MLO-Y4 cells as compared to cells treated with a scrambled siRNA control. **C** Primary osteocytes isolated from Sptbn1 CKO mice subjected to 5 min of fluid shear ( $30 \text{ dynes/cm}^2$ ) exhibited a nearly significant trend ( $p = 0.050$ ) for increased post-wounding cell death as compared to cells from WT mice. Bars in graphs in **B** and **C** show mean  $\pm$  SEM for each group, and each black circle represents an independent biological replicate experiment

differences were observed between Control and High Runner groups in tibial BMD ( $p_{\text{selection}} = 0.4998$ ) (Supplemental Fig. 1A), but mice with wheel access had lower tibial BMD values than those without ( $p_{\text{wheel}} = 0.0457$ ) and females had lower tibial BMD values than males ( $p_{\text{sex}} = 0.0195$ ) (Supplemental Fig. 1A).

For the femur, short-term wheel access did not generally impact cortical bone geometry as measured by microCT (Supplemental Table 1A) or cortical bone dynamic histomorphometry (Supplemental Table 1B). High Runner mice showed a significant increase in femoral cortical bone area ( $p_{\text{selection}} = 0.0185$ ) but not femoral cortical bone thickness ( $p_{\text{selection}} = 0.3776$ ) as compared to controls (Supplemental Table 1A). Female mice showed higher rates of femoral endocortical mineralizing surface than males ( $p_{\text{sex}} = 0.0312$ ), and somewhat surprisingly, High Runner mice demonstrated reductions in femoral endocortical mineralizing surface as

compared to controls ( $p_{\text{selection}} = 0.0100$ ), but few other differences in dynamic indices of cortical bone formation were associated with group, sex, or wheel access in these studies, likely due to the very short duration of wheel access (Supplemental Table 1B). A summary of the mixed models SAS analyses for the wheel-running mouse datasets is available as Supplemental Table 2.

Since short-term wheel access did not generally impact cortical bone geometry, even in the High Runner mice selected for high voluntary wheel running activity, we decided to explore alternative models of mechanical loading with which to interrogate the role of Sptbn1 in osteocyte PMD formation and in skeletal responses to loading. We therefore established a uniaxial tibial loading model first using wildtype female CD-1 mice to directly test the impact of bone loading (without muscle involvement) in osteocyte PMD formation. One acute loading bout was

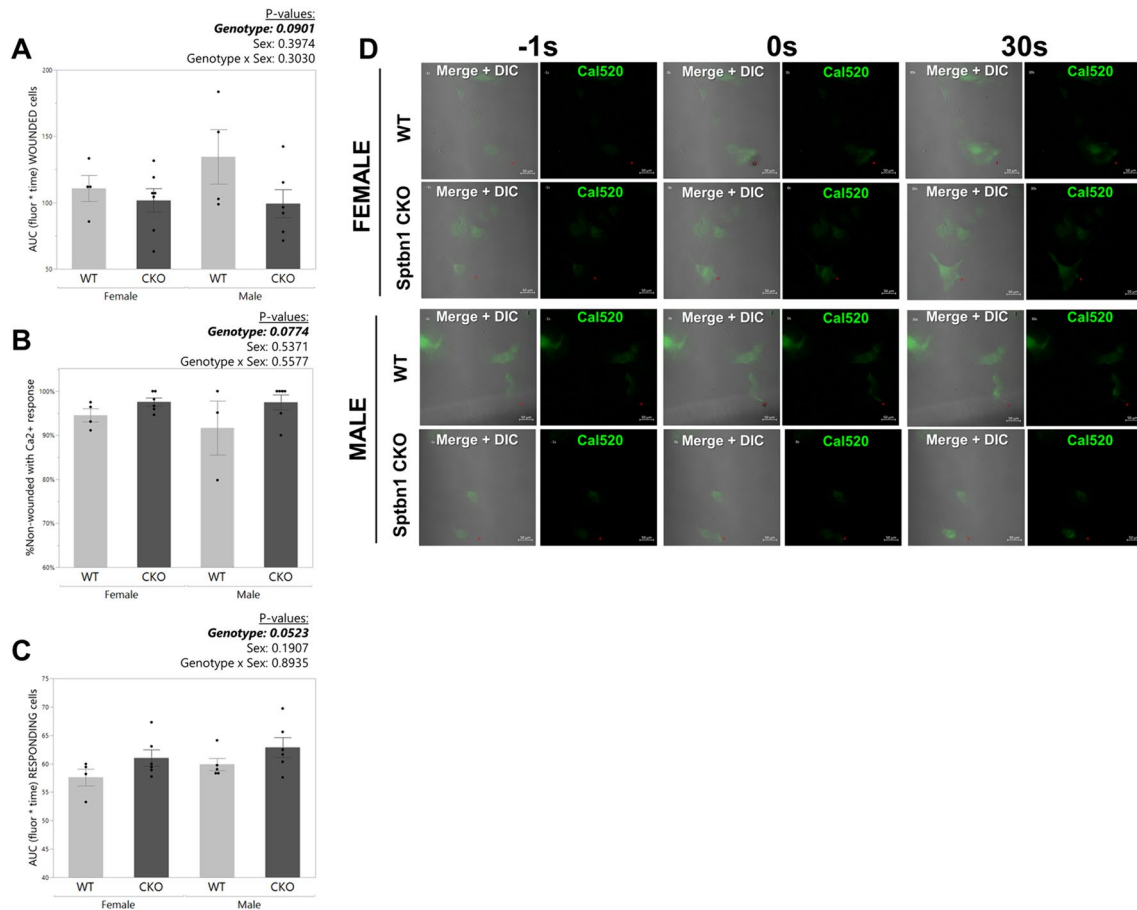


**Fig. 5** Calcium signaling in *Sptbn1* CKO and WT primary osteocytes initiated by laser wounding. Calcium signaling was studied via Cal-520AM fluorescence in primary osteocytes following creation of a laser-induced PMD on osteocyte dendritic processes via. **A** the area under the curve (AUC) for the Cal-520 fluorescence vs. time curve and **B**, **C** as Cal520 fluorescence in the neighboring, non-wounded

osteocytes in proximity to the wounded cell. Bars in graphs **A–C** show mean  $\pm$  SEM for each group; each black circle represents an independent biological replicate culture. **D** Representative images from the experiments shown in graphs **A–C**, captured at  $-1$  s before wounding,  $0$  s (i.e., at the time of wounding), and  $30$  s after wounding

associated with a significant ( $p = 0.0027$ ) increase in the number of osteocyte PMD in the loaded left limb as compared to the non-loaded right limb (Fig. 6C). This loading regimen, when repeated on alternating days for two weeks, significantly increased cortical bone thickness (Supplemental Fig. 2A) but not cortical bone area (Supplemental Fig. 2B). While periosteal mineral apposition rate was not increased by this protocol (Supplemental Fig. 2C), loading induced a significant increase in endocortical mineral apposition rate (Supplemental Fig. 2D) and periosteal and endocortical mineralizing surfaces (Supplemental Figs. 2E, H), supporting the osteogenic nature of our loading protocol. No evidence of woven bone formation was observed in any histological sections (Supplemental Fig. 2G, H), indicating that the loading protocol did not induce tissue-level skeletal damage. We therefore pursued further tibial loading studies with our *Sptbn1* CKO mouse line.

### ***Sptbn1* Deficiency Did Not Induce a Developmental Skeletal Phenotype but Blunted the Anabolic Response to Mechanical Loading**

Based on cellular phenotype observed from *Sptbn1* deficient osteocytes in response to mechanical loading, we anticipated the development of a skeletal phenotype in our *Sptbn1* CKO mouse model. Unexpectedly, the *Sptbn1* CKO mice did not demonstrate a skeletal phenotype, as measured by DXA, at 1 or 5 months of age (Supplemental Table 3). MicroCT analysis of bone architecture confirmed the lack of a developmental (sedentary) cortical bone phenotype at 5 months of age (Supplemental Table 4). Mice were then subjected to uniaxial tibial loading, as described above, for 2 weeks beginning at 12 weeks of age as in preliminary studies. Consistent with the lack of a developmental skeletal phenotype, there were no differences in cortical bone architecture between either male or female

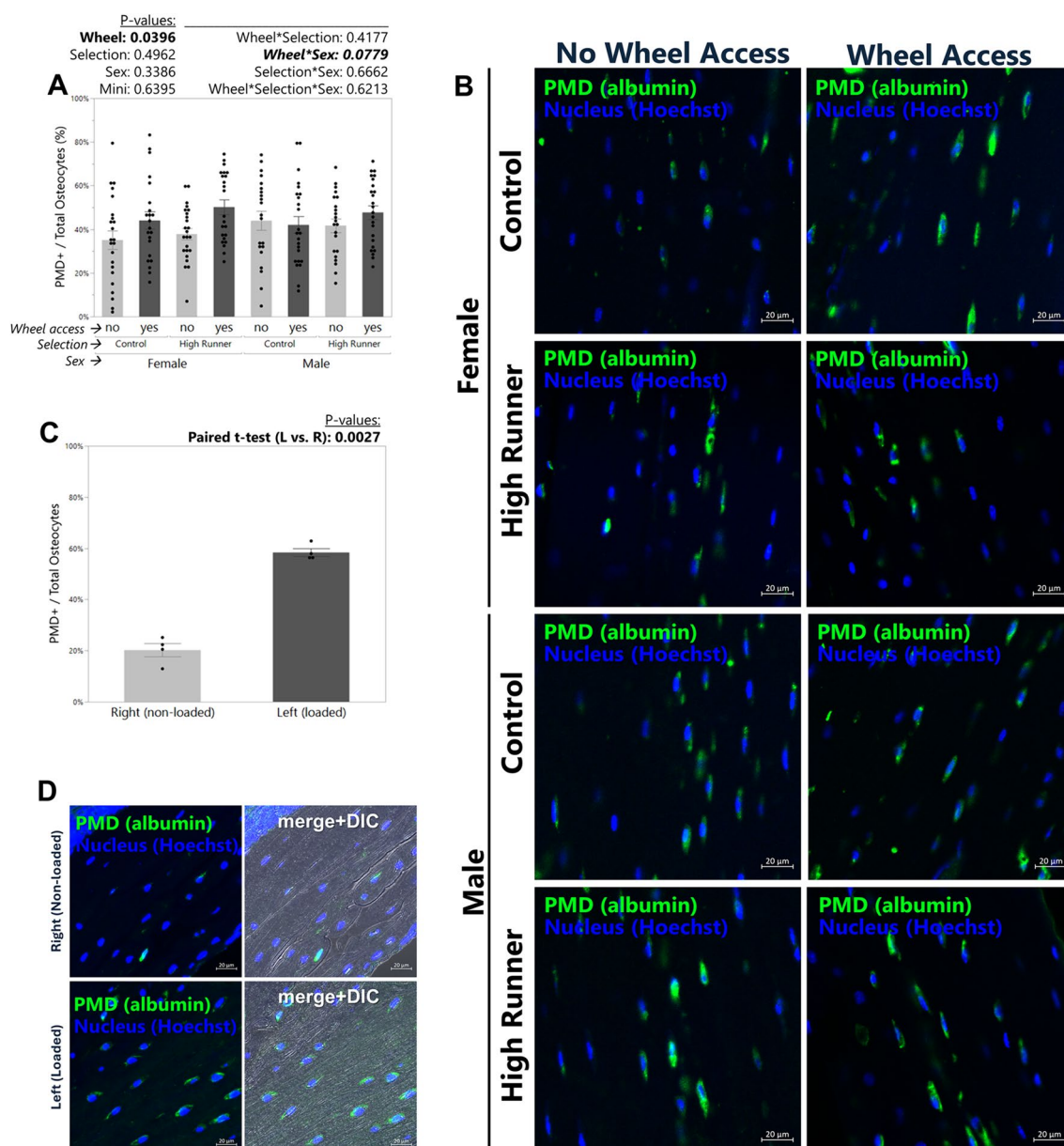


**Fig. 6** PMD formation from voluntary wheel running and uniaxial tibial loading. **A** Osteocyte PMD were detected via immunohistochemical staining to detect cytosolic endogenous mouse albumin in tibias from male and female Control and High Runner mice that were either given access to a voluntary running wheel (wheel access: yes) or not provided access to a running wheel (wheel access: no) for 6 days prior to sacrifice. Wheel access increased PMD abundance. Bars in graphs show mean  $\pm$  SEM for each group; each black circle represents one mouse. Groups were compared with 3-way ANOVA with 2-way interaction effects. **B** Representative images showing endogenous albumin (green) staining in tibias from male and female

Control and High Runner mice with or without access to a running wheel quantified in Panel A. **C** Osteocyte PMD were detected via immunohistochemical staining to detect cytosolic endogenous mouse albumin in tibias from female CD-1 mice subjected to a single bout of uniaxial tibial loading. Bars in graphs show mean  $\pm$  SEM for each limb; each black circle represents one mouse. Left vs. right sides were compared for each mouse using paired *t* tests. **D** Representative images showing endogenous albumin (green) staining in osteocytes in tibial sections from CD-1 mice exposed to a single bout of uniaxial loading quantified in Panel C

Sptbn1 CKO and WT littermate mice in the non-loaded right tibia ( $p_{\text{genotype}} > 0.310$ ; Supplemental Fig. 3). However, when subjected to 2 weeks of osteogenic loading, although Sptbn1 CKO mice tended to show an osteogenic response to loading (Supplemental Table 5), Sptbn1

CKO mice showed a significantly lower percent increase in cortical bone thickness between the loaded left tibia as compared to the non-loaded right tibia ( $p_{\text{genotype}} = 0.0153$ ; Fig. 7A–C, Supplemental Table 5), suggesting impaired cortical bone accrual with loading. Analyzing this same

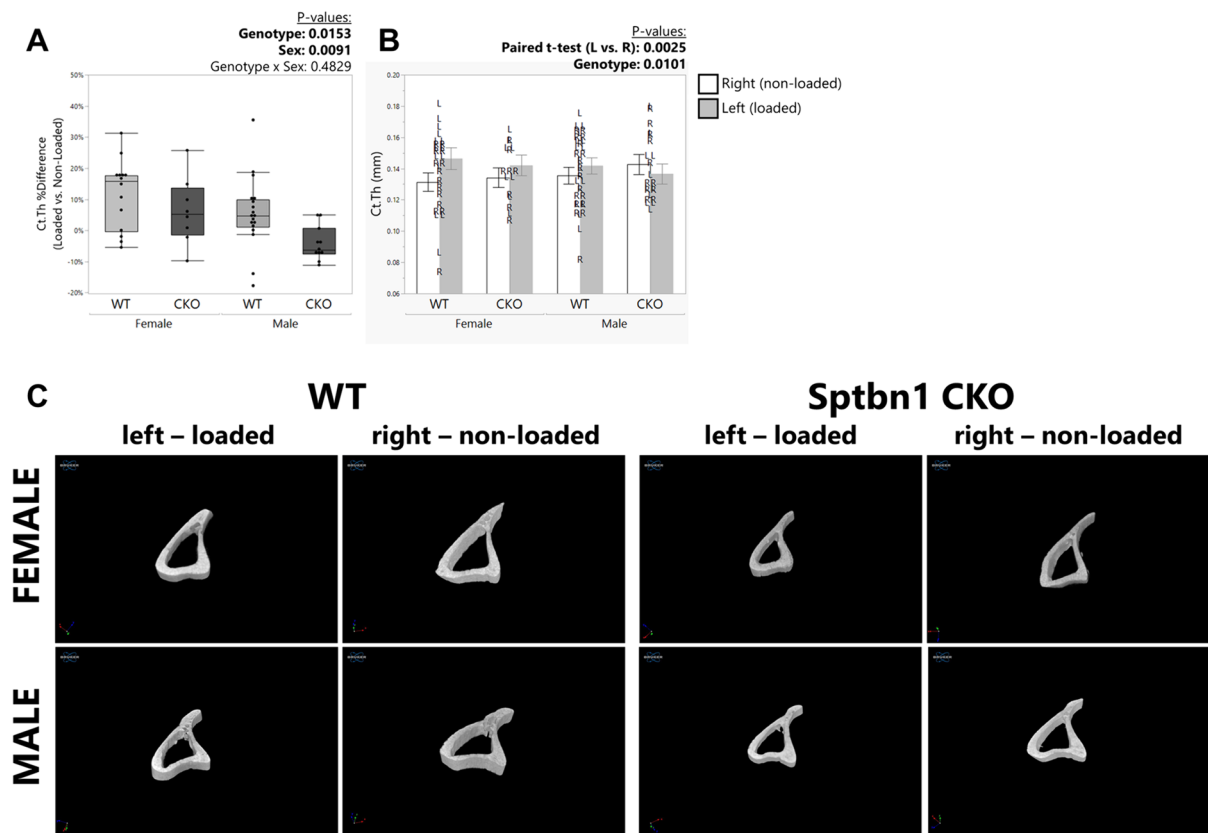


**Fig. 7** Blunted increase in cortical bone thickness with uniaxial tibial loading in *Sptbn1* CKO mice. **A** Micro-computed tomography was used to measure cortical bone thickness in the left and right tibia of each mouse. The percent difference in cortical thickness between the loaded and non-loaded limb was calculated for each mouse as: % difference  $Ct.Th = [Ct.Th \text{ left tibia} - Ct.Th \text{ right tibia}] / Ct.Th \text{ right tibia}$ . The relative increase in *Ct.Th* for the loaded left limb was blunted in *Sptbn1* CKO mice, shown by a significant effect of genotype in 2-way ANOVA ( $p = 0.0153$ ). Boxes in the graph show median, quartiles and outlier fences for each dataset. Each data point (black cir-

cle) represents one mouse. **B** Paired *t* tests were also used to compare cortical bone thickness between the loaded left limb and the non-loaded right limb for each *Sptbn1* CKO and WT mouse. Uniaxial tibial loading induced a significant increase in *Ct.Th*, shown by a significant *p*-value for paired *t* tests ( $p = 0.0025$ ), and when grouped by genotype, the *Sptbn1* CKO mice showed a lower relative increase in *Ct.Th* as compared to the WT animals ( $p = 0.0101$ ). Bars in graphs **B** show mean  $\pm$  SEM for each group, and each symbol shown represents the left (L) and right (R) tibia from one mouse. **C** Representative microCT reconstructions for samples shown in Panel **A**

dataset in another way, paired *t*-tests comparing the loaded left vs. non-loaded right tibia for each animal revealed a significant effect of loading ( $p_{\text{paired } t\text{-test}} = 0.0025$ ), as expected from our preliminary studies with CD-1 mice, but when grouped by genotype, *Sptbn1* CKO mice showed a blunted response ( $p_{\text{genotype}} = 0.0101$ ) (Fig. 7B, C, Supplemental Table 5). Loading-induced increases in other cortical bone properties, such as cortical bone area were not impacted by genotype (Supplemental Fig. 4A, B, Supplemental Table 5). Similarly, dynamic histomorphometric indices of cortical bone formation showed a significant effect of loading, consistent with our preliminary studies with CD-1 mice but were not impacted by genotype (Supplemental Fig. 4C–H). As in the preliminary studies with CD-1 mice, no evidence of woven bone formation was observed in any histological sections (*data not shown*).

### ***Sptbn1* CKO Mice Showed More Empty Osteocyte Lacunae After 2 Weeks of In Vivo Loading**

As our *in vitro* studies showed increased PMD abundance when *Sptbn1* was disrupted (Fig. 2), we anticipated increased prevalence of PMD formation in *Sptbn1* CKO mice subjected to one bout of acute mechanical loading *in vivo*. Interestingly, we did not observe an increased relative abundance of PMD created from one *in vivo* acute loading bout for the *Sptbn1* CKO mice (Fig. 8A, B). This discrepancy could reflect a difference in ability to visualize PMD in tissue sections as compared to cell culture conditions or could also reflect the fact that a repair failure can lead to loss of the intracellular PMD tracer [20, 50], as shown in our *in vitro* studies where dead cells did not retain fluorescent dextran (Fig. 4). As we observed increased cell

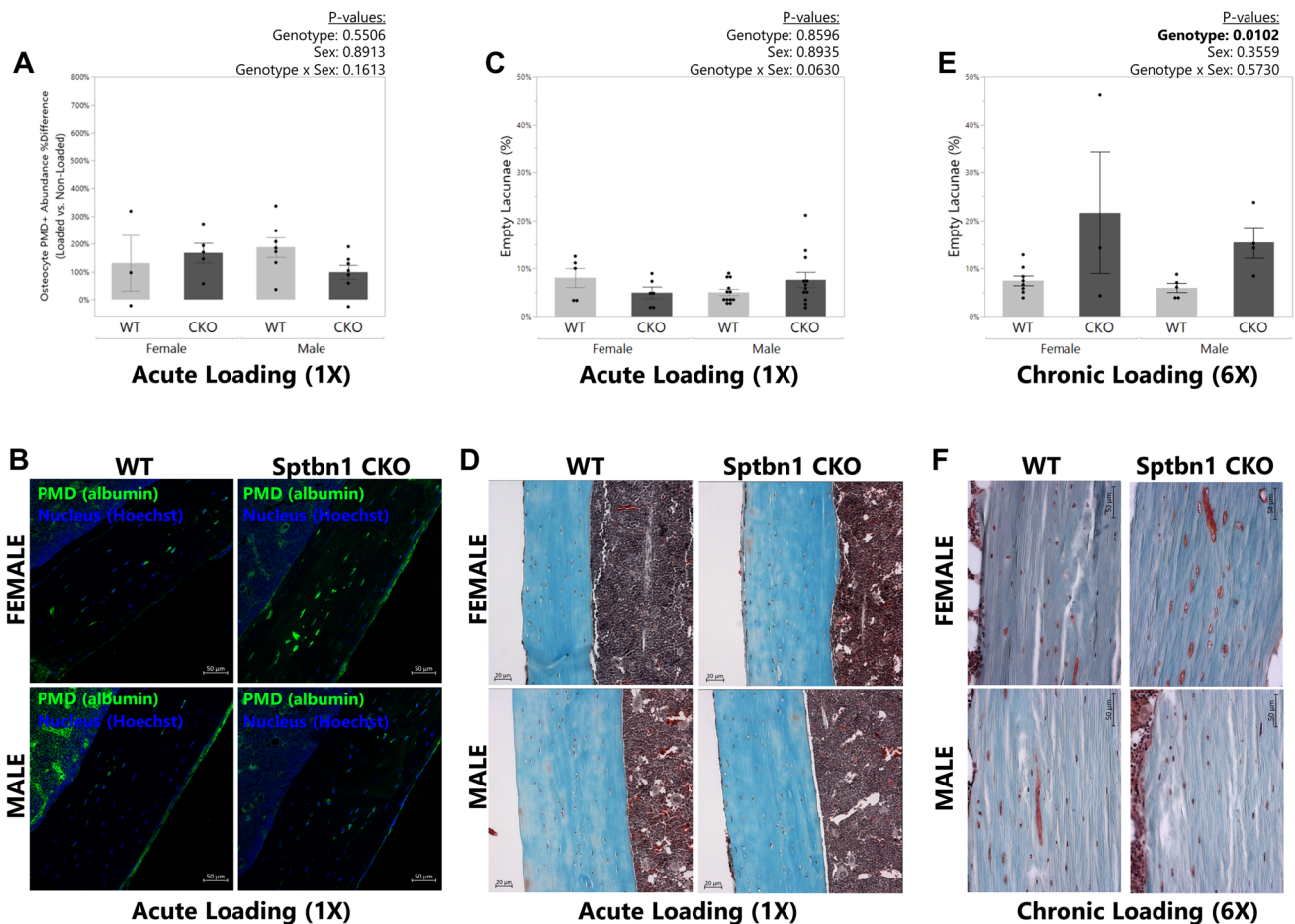


**Fig. 8** **A** Although PMD were increased by acute loading ( $p$  paired  $t$  test left vs. right < 0.0001; not shown), the relative difference in PMD abundance between the loaded left limb and non-loaded right limb was not different between *Sptbn1* CKO and WT mice (genotype = 0.5506). Bars in graph show mean  $\pm$  SEM for each group; each black circle represents one mouse. **B** Representative images showing endogenous albumin quantified in panel A. **C–F** Osteocyte lacunae vacancy in *Sptbn1* CKO and WT mice subjected to acute or chronic uniaxial tibial loading. The relative number of empty osteocyte lacunae

normalized to the total number of osteocyte lacunae was quantified in longitudinal sections loaded left tibias stained with Goldner's Trichrome. While no differences in the relative abundance of empty osteocyte lacunae were observed in mice subjected to one acute tibial loading bout (**C, D**;  $p = 0.8596$ ), both male and female *Sptbn1* CKO mice showed more empty lacunae after 2 weeks of chronic loading (**E, F**; 6 loading bouts), as shown by a significant effect of genotype in 2-way ANOVA ( $p = 0.0102$ ). Bars in graph show mean  $\pm$  SEM for each group; each black circle represents one mouse

death in *Sptbn1*-disrupted osteocytes subjected to loading in vitro (Fig. 4), we quantified osteocyte lacunar vacancy, measured as the number of empty lacunae relative to total lacunae number, in our tissue sections. This analysis was performed for the loaded left tibias immediately after a single acute loading bout, but we also quantified osteocyte lacunar vacancy in our mice subjected to 2 weeks of chronic loading, as a previous study suggested that empty lacunae were only visualized 48 h after osteocyte necrosis had occurred [68]. While no differences in osteocyte lacunar vacancy were observed immediately after a single loading bout (Fig. 8C, D), *Sptbn1* CKO mice subjected to 2 weeks of tibial loading demonstrated a significant increase in the number of empty osteocyte lacunae as compared to WT littermates (Fig. 8E, F).

## Discussion

Osteocytes likely utilize a range of mechanisms to sense mechanical loads at varying levels of physiological stress, but previous studies suggest that high-level loading conditions can promote the formation of osteocyte PMD which initiate mechanotransduction events [18–21, 69]. Modeling studies support the idea that osteocytic processes may be exposed to shear stresses of more than 50 dynes/cm<sup>2</sup> in vivo [70, 71] and both previous studies [21] as well as results presented here suggest that PMD are readily formed at these levels of loading. Importantly, preceding reports demonstrated that the development of loading-induced PMD in osteocytes and other cell types can be experimentally modulated [69]. We initially reported that Vitamin E

deprivation promoted osteocyte PMD development in mice following mechanical loading (downhill treadmill running) by increasing the ROS production [19]. We also showed that increased ROS production and changes in pericellular matrix deposition affected PMD development with aging and were potentially implicated in age-related loss of osteocytes [20]. However, these studies were largely observational in nature; the goal of the current study was to experimentally modulate the integrity of the spectrin network in osteocytes to determine if increasing osteocyte cell membrane fragility would affect osteocytic responses to loading. Results presented here suggest that disrupting the spectrin network in osteocytes increased the propensity for PMD formation at a given level of loading and decreased the likelihood of post-wounding osteocyte survival.

Although the mechanisms used by osteocytes to respond to different intensities of loading are still debated, several points of consistency have emerged in previous literature. Fluid shear produces larger strains at the cellular level and greater downstream mechanotransduction responses (like nitric oxide release) as compared to mechanical strain on the extracellular matrix [72–74]. The dendritic processes inside canaliculi are exposed to the greatest shear stresses [70, 75], and the processes, rather than cell bodies, are the key site of mechanosensation in the osteocyte [7, 76, 77]. Both previous studies [33, 34] and results presented here demonstrate that  $\beta$ II-spectrin is highly expressed in osteocytic processes where PMD preferentially formed with loading [21]. Spectrin expression in osteocytes was previously linked to mechanotransduction events such as nitric oxide secretion and calcium signaling [34], with spectrin disruption via diamide treatment leading to increased nitric oxide release by osteocytes, whereas our calcium signaling studies did not show a significant effect of *Sptbn1* CKO genetic deletion on this early mechanotransduction event, despite a slight, non-significant tendency ( $p_{\text{genotype}} = 0.0774$ ) for *Sptbn1* deletion to promote calcium signaling transmission to non-wounded cells in close proximity to the wounded osteocyte. Also, while we recently reported that application of osteocyte PMD-inducing turbulent fluid shear stress [20] increases expression of Cox-2 in osteocytes [78], we also acknowledge the considerable limitation that the studies presented here did not specifically investigate the roles of *Sptbn1* and osteocyte PMD formation in more mechanistic responses to mechanical loading such as changes in Wnt signaling or osteocytic control of bone remodeling (e.g., Rankl/Opg expression). Future studies more closely focused on mechanotransduction events will be needed to fully define the role of *Sptbn1*, and PMD formation, in osteocytic responses to mechanical loading.

The *Sptbn1* locus has been identified in several human genome-wide association studies as being linked to bone mineral density [36, 79], as well as risk of fracture and

susceptibility to osteoporosis [80–84]. Further studies utilizing bone co-expression networks constructed from murine cortical bone data suggested that the *Sptbn1* locus was causal for regulation of bone mineral density [35]. A recent report by Xu et al. demonstrated that *Sptbn1* expression, as measured by immunostaining in the distal femur, was reduced in 9- vs. 3-month old C57BL/6 mice as well as in ovariectomized as compared to sham-operated female mice [85]. The authors further used viral methods to silence and overexpress *Sptbn1* in the bone niche in vivo, showing that further suppression of *Sptbn1* expression exacerbated osteopenic phenotypes while overexpression of *Sptbn1* promoted rescue [85]. These effects, however, were attributed to beneficial impacts in osteoblasts and endothelial cells, as *Sptbn1* expression positively regulated osteoblast proliferation and differentiation as well as expression of vascular endothelial growth factor [85]; effects on osteocytes, including osteocyte viability, were unfortunately not reported. As *Dmp1-Cre* is reported to show activity in osteoblasts as well as osteocytes [86, 87], we cannot exclude the possibility that the blunted anabolic response to mechanical loading in our *Dmp1-Cre Sptbn1* CKO mice was driven by osteoblastic, rather than osteocytic, populations. However, we note that we failed to see a cortical bone skeletal phenotype develop under baseline conditions (in the absence of applied mechanical loading), and the increased osteocyte lacunar vacancy in the chronically loaded (but not acutely loaded) limbs of *Sptbn1* CKO mice is consistent with the increased post-wounding cell death seen in our in vitro diamide-, *Sptbn1* siRNA- and *Sptbn1* CKO primary osteocyte studies. Although *Dmp1-Cre* is also reported to show appreciable expression in muscle [43], the uniaxial tibial loading model used here (which loads bone without requiring voluntary muscular contraction) was selected for study to negate some of this concern.

The role of osteocyte *Sptbn1* expression shown here is consistent with the effect of the spectrin family protein dystrophin in skeletal muscle, where changes in the organization or expression of cytoskeletal structural proteins can affect propensity for PMD development. Many studies have shown that myocytes are more susceptible to the development of PMD in the absence of dystrophin [32, 58, 62, 88]. Wheel-running studies using *mdx* dystrophic mice showed that the mean distance covered in individual running bouts was positively correlated with the abundance of myofibers with centrally located nuclei as well as metrics of recent acute muscle damage in quadriceps muscle [88]. We also initially tested a voluntary wheel-running model, showing that wheel access was associated with osteocyte PMD formation, but ultimately selected a tibial loading model to test the mechanical responses of the *Sptbn1* CKO mice given the latter model's robust ability to induce osteocyte PMD formation, induce cortical bone gain, address concerns about off-target expression of *Dmp1-Cre* in skeletal muscle, and

reduce the variability of individual mouse responses to wheel access [88].

In conclusion, building upon previous studies interrogating PMD formation in dystrophin-deficient *mdx* mouse models, we targeted the Sptbn1 network in osteocytes to alter osteocyte plasma membrane fragility and to test the downstream effects of this manipulation on mechanotransduction and bone adaptation. Disruption of Sptbn1 in osteocytes increased PMD formation from fluid shear stress and decreased post-wounding cell viability due to impaired PMD repair. Our in vivo experimental results suggest that while osteocyte-targeted Sptbn1 deficient mice do not develop a baseline skeletal phenotype at younger ages, they do show a loading-induced phenotype of blunted cortical bone gain following repeated bouts of mechanical loading associated with loss of osteocyte viability. Taken together, the in vitro and in vivo work presented here suggests an important role for both Sptbn1 and PMD in osteocyte mechanosensation and subsequent downstream bone adaptation to high-level mechanical loading. Understanding the role of PMD-related mechanisms and how they affect mechanotransduction responses in these cases of rapid bone degeneration may prove key to identifying therapeutic targets to prevent or reverse the unloading-induced bone loss.

**Supplementary Information** The online version contains supplementary material available at <https://doi.org/10.1007/s00223-024-01285-2>.

**Acknowledgements** This work was funded by the National Science Foundation (NSF BMMB #1727949 to MM-L; NSF IOS #2038528 to TG), NASA (NASA Space Biology Grant #80NSSC21K0274 to MM-L) and the NIH (S10 OD025177, P01 AG036675 Core B). The authors wish to acknowledge the Augusta University Electron Microscopy and Histology Core for histological specimen preparation and the Augusta University Cell Imaging Core for assistance with imaging-related experiments.

## Declarations

**Conflict of interest** Mackenzie L. Hagan, Anik Tuladhar, Kanglun Yu, Dima W. Alhamad, Husam Bensreti, Jennifer Dorn, Victor M. Piedra, Nicholas Cantu, Eric G. Stokes, Daniel Blumenthal, Rachel L. Roberts, Vanshika Balayan, Sarah M. Bass, Thomas Dickerson, Anabel Liyen Cartelle, Marlian Montesinos-Cartagena, Mohamed E. Awad, Alberto A. Castro, Theodore Garland, Jr., Marion A. Cooley, Maribeth Johnson, Mark W. Hamrick, Paul L. McNeil and Meghan E. McGee-Lawrence have no conflicts of interest.

**Human rights and informed consent** This research did not involve human participants, their data or biological material.

## References

- Gomez-Cabello A, Ara I, Gonzalez-Aguero A, Casajus JA, Vicente-Rodriguez G (2012) Effects of training on bone mass in older adults: a systematic review. *Sports Med* 42:301–325
- Kontulainen S, Sievanen H, Kannus P, Pasanen M, Vuori I (2003) Effect of long-term impact-loading on mass, size, and estimated strength of humerus and radius of female racquet-sports players: a peripheral quantitative computed tomography study between young and old starters and controls. *J Bone Miner Res: Off J Am Soc Bone Miner Res* 18:352–359
- LaMothe JM, Hamilton NH, Zernicke RF (2005) Strain rate influences periosteal adaptation in mature bone. *Med Eng Phys* 27:277–284
- Lima F, De Falco V, Baima J, Carazzato JG, Pereira RM (2001) Effect of impact load and active load on bone metabolism and body composition of adolescent athletes. *Med Sci Sports Exerc* 33:1318–1323
- Tam N, Santos-Concejero J, Tucker R, Lamberts RP, Micklesfield LK (2018) Bone health in elite Kenyan runners. *J Sports Sci* 36:456–461
- Batra N, Burra S, Siller-Jackson AJ, Gu S, Xia X, Weber GF, DeSimone D, Bonewald LF, Lafer EM, Sprague E, Schwartz MA, Jiang JX (2012) Mechanical stress-activated integrin alpha5beta1 induces opening of connexin 43 hemichannels. *Proc Natl Acad Sci USA* 109:3359–3364
- Burra S, Nicolella DP, Francis WL, Freitas CJ, Mueschke NJ, Poole K, Jiang JX (2010) Dendritic processes of osteocytes are mechanotransducers that induce the opening of hemichannels. *Proc Natl Acad Sci USA* 107:13648–13653
- Cheng B, Zhao S, Luo J, Sprague E, Bonewald LF, Jiang JX (2001) Expression of functional gap junctions and regulation by fluid flow in osteocyte-like MLO-Y4 cells. *J Bone Miner Res: Off J Am Soc Bone Miner Res* 16:249–259
- Cherian PP, Cheng B, Gu S, Sprague E, Bonewald LF, Jiang JX (2003) Effects of mechanical strain on the function of Gap junctions in osteocytes are mediated through the prostaglandin EP2 receptor. *J Biol Chem* 278:43146–43156
- Jiang JX, Cherian PP (2003) Hemichannels formed by connexin 43 play an important role in the release of prostaglandin E(2) by osteocytes in response to mechanical strain. *Cell Commun Adhes* 10:259–264
- Genetos DC, Kephart CJ, Zhang Y, Yellowley CE, Donahue HJ (2007) Oscillating fluid flow activation of gap junction hemichannels induces ATP release from MLO-Y4 osteocytes. *J Cell Physiol* 212:207–214
- Plotkin LI, Speacht TL, Donahue HJ (2015) Cx43 and mechanotransduction in bone. *Curr Osteoporos Rep* 13:67–72
- Cabahug-Zuckerman P, Stout RF Jr, Majeska RJ, Thi MM, Spray DC, Weinbaum S, Schaffler MB (2018) Potential role for a specialized beta3 integrin-based structure on osteocyte processes in bone mechanosensation. *J Orthop Res* 36:642–652
- McNamara LM, Majeska RJ, Weinbaum S, Friedrich V, Schaffler MB (2009) Attachment of osteocyte cell processes to the bone matrix. *Anat Rec* 292:355–363
- Lyons JS, Joca HC, Law RA, Williams KM, Kerr JP, Shi G, Khairallah RJ, Martin SS, Konstantopoulos K, Ward CW, Stains JP (2017) Microtubules tune mechanotransduction through NOX2 and TRPV4 to decrease sclerostin abundance in osteocytes. *Sci Signal* 10(506):eaan5748
- Sasaki F, Hayashi M, Mouri Y, Nakamura S, Adachi T, Nakashima T (2020) Mechanotransduction via the Piezo1-Akt pathway underlies Sost suppression in osteocytes. *Biochem Biophys Res Commun* 521:806–813
- Mikolajewicz N, Sehayek S, Wiseman PW, Komarova SV (2019) Transmission of mechanical information by purinergic signaling. *Biophys J* 116:2009–2022
- Mikolajewicz N, Zimmermann EA, Willie BM, Komarova SV (2018) Mechanically-stimulated ATP release from murine bone cells is regulated by a balance of injury and repair. *Elife* 7:e37812



19. Hagan ML, Bahraini A, Pierce JL, Bass SM, Yu K, Elsayed R, Elsalanty M, Johnson MH, McNeil A, McNeil PL, McGee-Lawrence ME (2018) Inhibition of osteocyte membrane repair activity via dietary vitamin E deprivation impairs osteocyte survival. *Calcif Tissue Int* 104:224
20. Hagan ML, Yu K, Zhu J, Vinson BN, Roberts RL, Montesinos Cartagena M, Johnson MH, Wang L, Isales CM, Hamrick MW, McNeil PL, McGee-Lawrence ME (2020) Decreased pericellular matrix production and selection for enhanced cell membrane repair may impair osteocyte responses to mechanical loading in the aging skeleton. *Aging Cell* 19:e13056
21. Yu K, Sellman DP, Bahraini A, Hagan ML, Elsherbini A, Vanpelt KT, Marshall PL, Hamrick MW, McNeil A, McNeil PL, McGee-Lawrence ME (2018) Mechanical loading disrupts osteocyte plasma membranes which initiates mechanosensation events in bone. *J Orthop Res* 36:653–662
22. Clarke MS, Caldwell RW, Chiao H, Miyake K, McNeil PL (1995) Contraction-induced cell wounding and release of fibroblast growth factor in heart. *Circ Res* 76:927–934
23. Cooper ST, McNeil PL (2015) Membrane repair: mechanisms and pathophysiology. *Physiol Rev* 95:1205–1240
24. Grembowicz KP, Sprague D, McNeil PL (1999) Temporary disruption of the plasma membrane is required for c-fos expression in response to mechanical stress. *Mol Biol Cell* 10:1247–1257
25. Hamrick MW, McNeil PL, Patterson SL (2010) Role of muscle-derived growth factors in bone formation. *J Musculoskelet Neuronal Interact* 10:64–70
26. Howard AC, McNeil AK, McNeil PL (2011) Promotion of plasma membrane repair by vitamin E. *Nat Commun* 2:597
27. Howard AC, McNeil AK, Xiong F, Xiong WC, McNeil PL (2011) A novel cellular defect in diabetes: membrane repair failure. *Diabetes* 60:3034–3043
28. Labazi M, McNeil AK, Kurtz T, Lee TC, Pegg RB, Angeli JP, Conrad M, McNeil PL (2015) The antioxidant requirement for plasma membrane repair in skeletal muscle. *Free Radic Biol Med* 84:246–253
29. McNeil PL, Ito S (1989) Gastrointestinal cell plasma membrane wounding and resealing in vivo. *Gastroenterology* 96:1238–1248
30. McNeil PL, Khakee R (1992) Disruptions of muscle fiber plasma membranes. Role in exercise-induced damage. *Am J Pathol* 140:1097–1109
31. Yu QC, McNeil PL (1992) Transient disruptions of aortic endothelial cell plasma membranes. *Am J Pathol* 141:1349–1360
32. Bansal D, Miyake K, Vogel SS, Groh S, Chen CC, Williamson R, McNeil PL, Campbell KP (2003) Defective membrane repair in dysferlin-deficient muscular dystrophy. *Nature* 423:168–172
33. Kamioka H, Sugawara Y, Honjo T, Yamashiro T, Takano-Yamamoto T (2004) Terminal differentiation of osteoblasts to osteocytes is accompanied by dramatic changes in the distribution of actin-binding proteins. *J Bone Miner Res: Off J Am Soc Bone Miner Res* 19:471–478
34. Wu XT, Sun LW, Yang X, Ding D, Han D, Fan YB (2017) The potential role of spectrin network in the mechanotransduction of MLO-Y4 osteocytes. *Sci Rep* 7:40940
35. Calabrese GM, Mesner LD, Stains JP, Tommasini SM, Horowitz MC, Rosen CJ, Farber CR (2017) Integrating GWAS and Co-expression network data identifies bone mineral density genes SPTBN1 and MARK3 and an osteoblast functional module. *Cell Syst* 4(46–59):e44
36. Chen YC, Guo YF, He H, Lin X, Wang XF, Zhou R, Li WT, Pan DY, Shen J, Deng HW (2016) Integrative analysis of genomics and transcriptome data to identify potential functional genes of BMDs in females. *J Bone Miner Res: Off J Am Soc Bone Miner Res* 31:1041–1049
37. Hu Y, Tan LJ, Chen XD, Liu Z, Min SS, Zeng Q, Shen H, Deng HW (2017) Identification of novel potentially-pleiotropic variants associated with osteoporosis and obesity using cFDR method. *J Clin Endocrinol Metab* 103:125
38. Stern AR, Stern MM, Van Dyke ME, Jahn K, Prideaux M, Bonewald LF (2012) Isolation and culture of primary osteocytes from the long bones of skeletally mature and aged mice. *Biotechniques* 52:361–373
39. McGee-Lawrence ME, Carpio LR, Schulze RJ, Pierce JL, McNiven MA, Farr JN, Khosla S, Oursler MJ, Westendorf JJ (2016) Hdac3 deficiency increases marrow adiposity and induces lipid storage and glucocorticoid metabolism in osteochondroprogenitor cells. *J Bone Miner Res: Off J Am Soc Bone Miner Res* 31:116–128
40. Archer JD, Vargas CC, Anderson JE (2006) Persistent and improved functional gain in mdx dystrophic mice after treatment with L-arginine and deflazacort. *FASEB J: Off Publ Fed Am Soc Exp Biol* 20:738–740
41. Meek TH, Lonquich BP, Hannon RM, Garland T (2009) Endurance capacity of mice selectively bred for high voluntary wheel running. *J Exp Biol* 212:2908–2917
42. Khan RH, Rhodes JS, Girard IA, Schwartz NE, Garland TG (2024) Does behavior evolve first? Correlated responses to selection for voluntary wheel-running behavior in house mice. *Ecol Evol Physiol* 97:97–117
43. Dasgupta K, Lessard S, Hann S, Fowler ME, Robling AG, Warman ML (2021) Sensitive detection of Cre-mediated recombination using droplet digital PCR reveals Tg(BGLAP-Cre) and Tg(DMP1-Cre) are active in multiple non-skeletal tissues. *Bone* 142:115674
44. Pead MJ, Suswillo R, Skerry TM, Vedi S, Lanyon LE (1988) Increased 3H-uridine levels in osteocytes following a single short period of dynamic bone loading in vivo. *Calcif Tissue Int* 43:92–96
45. Skerry TM, Bitensky L, Chayen J, Lanyon LE (1988) Loading-related reorientation of bone proteoglycan in vivo. Strain memory in bone tissue? *J Orthop Res* 6:547–551
46. de Souza RL, Pitsillides AA, Lanyon LE, Skerry TM, Chenu C (2005) Sympathetic nervous system does not mediate the load-induced cortical new bone formation. *J Bone Miner Res* 20:2159–2168
47. Pierce JL, Sharma AK, Roberts RL, Yu K, Irsik DL, Choudhary V, Dorn JS, Bensreti H, Benson RD Jr, Kaiser H, Khayrullin A, Davis C, Wehrle CJ, Johnson MH, Bollag WB, Hamrick MW, Shi X, Isales CM, McGee-Lawrence ME (2022) The glucocorticoid receptor in osterix-expressing cells regulates bone mass, bone marrow adipose tissue, and systemic metabolism in female mice during aging. *J Bone Miner Res: Off J Am Soc Bone Miner Res* 37:285–302
48. Pierce JL, Ding KH, Xu J, Sharma AK, Yu K, Del Mazo AN, Rodriguez-Santos Z, Bernard P, Bollag WB, Johnson MH, Hamrick MW, Begun DL, Shi XM, Isales CM, McGee-Lawrence ME (2019) The glucocorticoid receptor in osteoprogenitors regulates bone mass and marrow fat. *J Endocrinol* 243:27
49. McGee MEMA, Johnson SE, Nelson OL, Robbins CT, Donahue SW (2008) Increased bone turnover with balanced resorption and formation prevent cortical bone loss during disuse (hibernation) in grizzly bears (*Ursus arctos horribilis*). *Bone* 42:396
50. Hagan ML, Bahraini A, Pierce JL, Bass SM, Yu K, Elsayed R, Elsalanty M, Johnson MH, McNeil A, McNeil PL, McGee-Lawrence ME (2019) Inhibition of osteocyte membrane repair activity via dietary vitamin E deprivation impairs osteocyte survival. *Calcif Tissue Int* 104:224–234
51. Dempster DW, Compston JE, Drezner MK, Glorieux FH, Kanis JA, Malluche H, Meunier PJ, Ott SM, Recker RR, Parfitt AM (2013) Standardized nomenclature, symbols, and units for bone histomorphometry: a 2012 update of the report of the ASBMR

- histomorphometry nomenclature committee. *J Bone Miner Res: Off J Am Soc Bone Miner Res* 28:2–17
52. Grubbs FE (1969) Procedures for detecting outlying observations in samples. *Technometrics* 11:1–21
  53. Wallace IJ, Tommasini SM, Judex S, Garland T Jr, Demes B (2012) Genetic variations and physical activity as determinants of limb bone morphology: an experimental approach using a mouse model. *Am J Phys Anthropol* 148:24–35
  54. Garland T Jr, Morgan MT, Swallow JG, Rhodes JS, Girard I, Belter JG, Carter PA (2002) Evolution of a small-muscle polymorphism in lines of house mice selected for high activity levels. *Evolution* 56:1267–1275
  55. Houle-Leroy P, Guderley H, Swallow JG, Garland T Jr (2003) Artificial selection for high activity favors mighty mini-muscles in house mice. *Am J Physiol Regul Integr Comp Physiol* 284:R433–443
  56. Kelly SA, Bell TA, Selitsky SR, Buus RJ, Hua K, Weinstock GM, Garland T Jr, Pardo-Manuel de Villena F, Pomp D (2013) A novel intronic single nucleotide polymorphism in the myosin heavy polypeptide 4 gene is responsible for the mini-muscle phenotype characterized by major reduction in hind-limb muscle mass in mice. *Genetics* 195:1385–1395
  57. Erickson HP (2009) Size and shape of protein molecules at the nanometer level determined by sedimentation, gel filtration, and electron microscopy. *Biol Proced Online* 11:32–51
  58. Clafflin DR, Brooks SV (2008) Direct observation of failing fibers in muscles of dystrophic mice provides mechanistic insight into muscular dystrophy. *Am J Physiol Cell Physiol* 294:C651–658
  59. De Luca A, Pierno S, Liantonio A, Cetrone M, Camerino C, Frayssé B, Mirabella M, Servidei S, Ruegg UT, Conte Camerino D (2003) Enhanced dystrophic progression in mdx mice by exercise and beneficial effects of taurine and insulin-like growth factor-1. *J Pharmacol Exp Ther* 304:453–463
  60. Weller B, Karpati G, Carpenter S (1990) Dystrophin-deficient mdx muscle fibers are preferentially vulnerable to necrosis induced by experimental lengthening contractions. *J Neurol Sci* 100:9–13
  61. Quinlan JG, Wong BL, Niemeier RT, McCullough AS, Levin L, Emanuele M (2006) Poloxamer 188 failed to prevent exercise-induced membrane breakdown in mdx skeletal muscle fibers. *Neuromuscul Disord* 16:855–864
  62. Clarke MS, Khakee R, McNeil PL (1993) Loss of cytoplasmic basic fibroblast growth factor from physiologically wounded myofibers of normal and dystrophic muscle. *J Cell Sci* 106(Pt 1):121–133
  63. Moraska A, Deak T, Spencer RL, Roth D, Fleshner M (2000) Treadmill running produces both positive and negative physiological adaptations in Sprague-Dawley rats. *Am J Physiol Regul Integr Comp Physiol* 279:R1321–1329
  64. Park KS, Lee MG (2015) Effects of unaccustomed downhill running on muscle damage, oxidative stress, and leukocyte apoptosis. *J Exerc Nutrition Biochem* 19:55–63
  65. Rice H, Kurz M, Mai P, Robertz L, Bill K, Derrick TR, Willwacher S (2024) Speed and surface steepness affect internal tibial loading during running. *J Sport Health Sci* 13:118–124
  66. Suito H, Fujikawa K, Ohsako M (2023) Eccentric contractions during downhill running induce Osgood-Schlatter disease in the tibial tuberosity in rats: a focus on histological structures. *Sci Rep* 13:9863
  67. Garland T Jr, Kelly SA, Malisch JL, Kolb EM, Hannon RM, Keeney BK, Van Cleave SL, Middleton KM (2011) How to run far: multiple solutions and sex-specific responses to selective breeding for high voluntary activity levels. *Proc Biol Sci* 278:574–581
  68. Tatsumi S, Ishii K, Amizuka N, Li M, Kobayashi T, Kohno K, Ito M, Takeshita S, Ikeda K (2007) Targeted ablation of osteocytes induces osteoporosis with defective mechanotransduction. *Cell Metab* 5:464–475
  69. Hagan ML, Balayan V, McGee-Lawrence ME (2021) Plasma membrane disruption (PMD) formation and repair in mechanosensitive tissues. *Bone* 149:115970
  70. Price C, Zhou X, Li W, Wang L (2011) Real-time measurement of solute transport within the lacunar-canalicular system of mechanically loaded bone: direct evidence for load-induced fluid flow. *J Bone Miner Res: Off J Am Soc Bone Miner Res* 26:277–285
  71. Verbruggen SW, Vaughan TJ, McNamara LM (2014) Fluid flow in the osteocyte mechanical environment: a fluid-structure interaction approach. *Biomech Model Mechanobiol* 13:85–97
  72. Smalt R, Mitchell FT, Howard RL, Chambers TJ (1997) Induction of NO and prostaglandin E2 in osteoblasts by wall-shear stress but not mechanical strain. *Am J Physiol* 273:E751–758
  73. McGarry JG, Klein-Nulend J, Mullender MG, Prendergast PJ (2005) A comparison of strain and fluid shear stress in stimulating bone cell responses—a computational and experimental study. *FASEB J: Off Publ Fed Am Soc Exp Biol* 19:482–484
  74. Ganesh T, Laughrey LE, Niroobaksh M, Lara-Castillo N (2020) Multiscale finite element modeling of mechanical strains and fluid flow in osteocyte lacunocanalicular system. *Bone* 137:115328
  75. Anderson EJ, Kaliyamoorthy S, Iwan J, Alexander D, Knothe Tate ML (2005) Nano-microscale models of periosteocytic flow show differences in stresses imparted to cell body and processes. *Ann Biomed Eng* 33:52–62
  76. Thi MM, Suadicani SO, Schaffler MB, Weinbaum S, Spray DC (2013) Mechanosensory responses of osteocytes to physiological forces occur along processes and not cell body and require alphaVbeta3 integrin. *Proc Natl Acad Sci USA* 110:21012–21017
  77. Wu D, Schaffler MB, Weinbaum S, Spray DC (2013) Matrix-dependent adhesion mediates network responses to physiological stimulation of the osteocyte cell process. *Proc Natl Acad Sci USA* 110:12096–12101
  78. Tuladhar A, Shaver JC, McGee WA, Yu K, Dorn J, Horne JL, Alhamad DW, Hagan ML, Cooley MA, Zhong R, Bollag W, Johnson M, Hamrick MW, McGee-Lawrence ME (2024) Prkd1 regulates the formation and repair of plasma membrane disruptions (PMD) in osteocytes. *Bone* 186:117147
  79. Rivadeneira F, Styrkarsdottir U, Estrada K, Halldorsson BV, Hsu YH, Richards JB, Zillikens MC, Kavvoura FK, Amin N, Aulchenko YS, Cupples LA, Deloukas P, Demissie S, Grundberg E, Hofman A, Kong A, Karasik D, van Meurs JB, Oostra B, Pastinen T, Pols HA, Sigurdsson G, Soranzo N, Thorleifsson G, Thorsteinsdottir U, Williams FM, Wilson SG, Zhou Y, Ralston SH, van Duijn CM, Spector T, Kiel DP, Stefansson K, Ioannidis JP, Uitterlinden AG (2009) Twenty bone-mineral-density loci identified by large-scale meta-analysis of genome-wide association studies. *Nat Genet* 41:1199–1206
  80. Estrada K, Styrkarsdottir U, Evangelou E, Hsu YH, Duncan EL, Ntzani EE, Oei L, Albagha OM, Amin N, Kemp JP, Koller DL, Li G, Liu CT, Minster RL, Moayyeri A, Vandenput L, Willner D, Xiao SM, Yerges-Armstrong LM, Zheng HF, Alonso N, Eriksson J, Kammerer CM, Kaptoge SK, Leo PJ, Thorleifsson G, Wilson SG, Wilson JF, Aalto V, Alen M, Aragaki AK, Aspelund T, Center JR, Dailiana Z, Duggan DJ, Garcia M, Garcia-Giralt N, Giroux S, Hallmans G, Hocking LJ, Husted LB, Jameson KA, Khusainova R, Kim GS, Kooperberg C, Koromila T, Kruk M, Laaksonen M, Lacroix AZ, Lee SH, Leung PC, Lewis JR, Masi L, Mencej-Bedrac S, Nguyen TV, Noguez X, Patel MS, Prezelj J, Rose LM, Scollen S, Siggeirsdottir K, Smith AV, Svensson O, Trompet S, Trummer O, van Schoor NM, Woo J, Zhu K, Balcells S, Brandi ML, Buckley BM, Cheng S, Christiansen C, Cooper C, Dedoussis G, Ford I, Frost M, Goltzman D, Gonzalez-Macias J, Kahonen M, Karlsson M, Khusnutdinova E, Koh JM, Kollia P, Langdahl BL, Leslie WD, Lips P, Ljunggren O, Lorenc RS, Marc J, Mellstrom

- D, Obermayer-Pietsch B, Olmos JM, Pettersson-Kymmer U, Reid DM, Riancho JA, Ridker PM, Rousseau F, Slagboom PE, Tang NL et al (2012) Genome-wide meta-analysis identifies 56 bone mineral density loci and reveals 14 loci associated with risk of fracture. *Nat Genet* 44:491–501
81. Liu JM, Zhang MJ, Zhao L, Cui B, Li ZB, Zhao HY, Sun LH, Tao B, Li M, Ning G (2010) Analysis of recently identified osteoporosis susceptibility genes in Han Chinese women. *J Clin Endocrinol Metab* 95:E112–120
  82. Moayeri A, Hsu YH, Karasik D, Estrada K, Xiao SM, Nielson C, Srikanth P, Giroux S, Wilson SG, Zheng HF, Smith AV, Pye SR, Leo PJ, Teumer A, Hwang JY, Ohlsson C, McGuigan F, Minster RL, Hayward C, Olmos JM, Lyytikäinen LP, Lewis JR, Swart KM, Masi L, Oldmeadow C, Holliday EG, Cheng S, van Schoor NM, Harvey NC, Kruk M, del Greco MF, Igl W, Trummer O, Grigoriou E, Luben R, Liu CT, Zhou Y, Oei L, Medina-Gomez C, Zmuda J, Tranah G, Brown SJ, Williams FM, Soranzo N, Jakobsdottir J, Siggeirsdottir K, Holliday KL, Hannemann A, Go MJ, Garcia M, Polasek O, Laaksonen M, Zhu K, Enneman AW, McEvoy M, Peel R, Sham PC, Jaworski M, Johansson A, Hicks AA, Pludowski P, Scott R, Dhonukshe-Rutten RA, van der Velde N, Kahonen M, Viikari JS, Sievanen H, Raitakari OT, Gonzalez-Macias J, Hernandez JL, Mellstrom D, Ljunggren O, Cho YS, Volker U, Nauck M, Homuth G, Volzke H, Haring R, Brown MA, McCloskey E, Nicholson GC, Eastell R, Eisman JA, Jones G, Reid IR, Dennison EM, Wark J, Boonen S, Vanderschueren D, Wu FC, Aspelund T, Richards JB, Bauer D, Hofman A, Khaw KT, Dedoussis G, Obermayer-Pietsch B, Gyllensten U, Pramstaller PP, Lorenc RS et al (2014) Genetic determinants of heel bone properties: genome-wide association meta-analysis and replication in the GEFOS/GENOMOS consortium. *Hum Mol Genet* 23:3054–3068
  83. Deng YH, Zhao L, Zhang MJ, Pan CM, Zhao SX, Zhao HY, Sun LH, Tao B, Song HD, Wang WQ, Ning G, Liu JM (2013) The influence of the genetic and non-genetic factors on bone mineral density and osteoporotic fractures in Chinese women. *Endocrine* 43:127–135
  84. Wang C, Zhang Z, Zhang H, He JW, Gu JM, Hu WW, Hu YQ, Li M, Liu YJ, Fu WZ, Yue H, Ke YH, Zhang ZL (2012) Susceptibility genes for osteoporotic fracture in postmenopausal Chinese women. *J Bone Miner Res: Off J Am Soc Bone Miner Res* 27:2582–2591
  85. Xu X, Yang J, Ye Y, Chen G, Zhang Y, Wu H, Song Y, Feng M, Feng X, Chen X, Wang X, Lin X, Bai X, Shen J (2021) SPTBN1 prevents primary osteoporosis by modulating osteoblasts proliferation and differentiation and blood vessels formation in bone. *Front Cell Dev Biol* 9:653724
  86. Xiong J, Piemontese M, Onal M, Campbell J, Goellner JJ, Dusevich V, Bonewald L, Manolagas SC, O'Brien CA (2015) Osteocytes, not osteoblasts or lining cells, are the main source of the RANKL required for osteoclast formation in remodeling bone. *PLoS ONE* 10:e0138189
  87. Lu Y, Xie Y, Zhang S, Dusevich V, Bonewald LF, Feng JQ (2007) DMP1-targeted Cre expression in odontoblasts and osteocytes. *J Dent Res* 86:320–325
  88. Smythe GM, White JD (2011) Voluntary wheel running in dystrophin-deficient (mdx) mice: relationships between exercise parameters and exacerbation of the dystrophic phenotype. *PLoS Curr* 3:RRN1295

**Publisher's Note** Springer Nature remains neutral with regard to jurisdictional claims in published maps and institutional affiliations.

Springer Nature or its licensor (e.g. a society or other partner) holds exclusive rights to this article under a publishing agreement with the author(s) or other rightsholder(s); author self-archiving of the accepted manuscript version of this article is solely governed by the terms of such publishing agreement and applicable law.